Bioorg. Med. Chem. 46 (2021) 116385

Contents lists available at ScienceDirect

Bioorganic & Medicinal Chemistry

journal homepage: www.elsevier.com/locate/bmc

Further SAR studies on natural template based neuroprotective molecules for the treatment of Alzheimer's disease

Yash Pal Singh [a], Gauri Shankar [a], Shagufta Jahan [b], Gourav Singh [a], Navneet Kumar [c], Atanu Barik [a,1], Prabhat Upadhyay [b], Lovejit Singh [a,2], Kajal Kamble [b], Gireesh Kumar Singh [d], Sanjay Tiwari [e], Prabha Garg [c], Sarika Gupta [b], Gyan Modi [a,*]

[a] Department of Pharmaceutical Engineering & Technology, Indian Institute of Technology (Banaras Hindu University), Varanasi 221005, India
[b] National Institute of Immunology, New Delhi 110067, India
[c] Department of Pharmacoinformatics, National Institute of Pharmaceutical Education and Research (NIPER), Sector 67, SAS Nagar 160062, India
[d] Department of Pharmacy, School of Health Science, Central University of South Bihar, Gaya 824236, India
[e] Department of Pharmaceutics, National Institute of Pharmaceutical Education and Research (NIPER) – Raebareli, Lucknow 226002, India

ARTICLE INFO

Keywords:
Alzheimer's disease
Ferulic acid
Cholinesterase inhibitors
Antioxidant
Iron chelator
Morris water maze

ABSTRACT

In our earlier paper, we described ferulic acid (**FA**) template based novel series of multifunctional cholinesterase (ChE) inhibitors for the management of AD. This report has further extended the structure–activity relationship (SAR) studies of this series of molecules in a calibrated manner to improve upon the ChEs inhibition and antioxidant property to identify the novel potent multifunctional molecules. To investigate the effect of replacement of phenylpiperazine ring with benzylpiperazine, increase in the linker length between **FA** and substituted phenyl ring, and replacement of indole moiety with tryptamine on this molecular template, three series of novel molecules were developed. All synthesized compounds were tested for their acetyl and butyryl cholinestrases (AChE and BChE) inhibitory properties. Enzyme inhibition and PAS binding studies identified compound **13b** as a lead molecule with potent inhibitor property towards AChE/BChE (AChE $IC_{50} = 0.96 \pm 0.14$ μM, BChE $IC_{50} = 1.23 \pm 0.23$ μM) compared to earlier identified lead molecule **EJMC-G** (AChE $IC_{50} = 5.74 \pm 0.13$ μM, BChE $IC_{50} = 14.05 \pm 0.10$ μM, respectively). Molecular docking and dynamics studies revealed that **13b** fits well into the active sites of AChE and BChE, forming stable and strong interactions with key residues Trp86, Ser125, Glu202, Trp 286, Phe295, Tyr 337 in AChE, and with Trp 82, Gly115, Tyr128, and Ser287 in BChE. The compound, **13b** was found to be three times more potent antioxidant in a DPPH assay ($IC_{50} = 20.25 \pm 0.26$ μM) over the earlier identified **EJMC-B** ($IC_{50} = 61.98 \pm 0.30$ μM) and it also was able to chelate iron. Co-treatment of **13b** with H_2O_2, significantly attenuated and reversed H_2O_2-induced toxicity in the SH-SY5Y cells. The parallel artificial membrane permeability assay-blood brain barrier (PAMPA-BBB) revealed that **13b** could cross BBB efficiently. Finally, the *in-vivo* efficacy of **13b** at dose of 10 mg/kg in scopolamine AD model has been demonstrated. The present study strongly suggests that the naturally inspired multifunctional molecule **13b** may behave as a potential novel therapeutic agent for AD management.

Abbreviations: ACh, acetylcholine; AChE, acetylcholinesterase; AD, Alzheimer's disease; BuChE, butyrylcholinesterase; **DPZ**, donepezil; **FA**, ferulic acid; PAS, peripheral anionic site; CAS, catalytic active site; ROS, reactive oxygen species; BBB, blood-brain barrier; hACh, human acetylcholine; DPPH, 2,2-diphenyl-1-picrylhydrazyl; MTT, 3- (4,5-dimethylthiazol-2-yl)-2,5-diphenyltetrazolium bromide; UV, ultraviolet; AFM, atomic force microscopy; MD, molecular dynamics; LogP, lipophilicity; TPSA, topological polar surface area; MW, molecular weight; HBD, hydrogen bond donors; HBA, hydrogen bond acceptors; RB, Rotatable bonds; BOC, *tert*-butyloxycarbonyl; DCM, dichloromethane; DIPEA, N-diisopropylethylamine; EDCI.HCl, 1-[3-(dimethyamino)-propyl]-3-ethylcarbodiimide hydrochloride; THF, tetrahydrofuran; HOBt, N-hydroxybenzotriazole, EtOAc, ethylacetate; TFA, trifluoroacetic acid; TLC, thin layer chromatography; $CDCl_3$, deuterated chloroform; DMSO-d_6, deuterated dimethyl sulfoxide-d_6; TMS, tetramethylsilane; Hz, hertz; HR-MS, high-resolution mass spectrometry; ATCI, acetylthiocholine iodide; BTCI, butyrylthiocholine iodide; DTNB, 5,5'-dithiobis-2-nitrobenzoic acid.

* Corresponding author at: Department of Pharmaceutical Engineering & Technology, Indian Institute of Technology (BHU), Rm # 23, Varanasi, UP 221005, India.
E-mail address: gpmodi.phe@itbhu.ac.in (G. Modi).
[1] Current address: Evalueserve SEZ Private Limited, 8th Floor, Building No:4, Candor Gurgaon One Realty Projects Pvt. Ltd-SEZ, Sector-48, Gurgaon, Haryana 122001, India.
[2] Current address: Mylan Laboratories Limited, Plot No. H, 12, MIDC, Industrial Area, Waluj, Aurangabad, Maharashtra 431136. India.

https://doi.org/10.1016/j.bmc.2021.116385
Received 4 April 2021; Received in revised form 2 August 2021; Accepted 23 August 2021
Available online 28 August 2021
0968-0896/© 2021 Elsevier Ltd. All rights reserved.

1. Introduction

Alzheimer's disease (AD) is a multifactorial progressive neurodegenerative disorder and the most common form of dementia worldwide. The symptoms associated with AD involve impairment in memory, language skills, personal behavior, and thinking.[1] These symptoms appear due to the neuronal damage not only limited to the brain's region responsible for the cognitive function but may extend to neurons in different parts of the brain. It is worth mentioning that dementia is the fifth-leading cause of death in the United States in people older than 65. As per 2020 AD facts and figures, the mortality rate in the last two decades due to stroke, HIV, and heart disease has decreased significantly, while 146.2% increase in deaths from AD has been reported.[2] As pre-WHO, around 50 million people worldwide live with dementia, and every year this number is escalating at a rapid rate.[3] The total cost for all individuals with AD and other dementia is expected to rise to approximately $1.1 trillion by 2050. The exact molecular mechanisms responsible for neurodegeneration in AD are not clear yet, however, there is a plethora of evidence, including publications from our research group, that AD is multifactorial.[4–9] The oldest hypothesis regarding AD pathophysiology is the "cholinergic hypothesis", suggesting the massive loss of cholinergic neurons in AD.[10,11] Acetylcholine (ACh) is one of the major neurotransmitters involved in learning and memory. The brain regions most affected by neuronal loss in AD are essentially made of cholinergic neurons, therefore, restoring physiological ACh level has been considered a viable therapy for AD.[12,13] Cholinesterases (ChEs) are responsible for the hydrolysis of ACh into choline and acetic acid. The two main types of ChEs: (i) acetylcholinesterase (AChE), and (ii) butyrylcholinesterase (BChE). AChE is one of the key enzymes that play a significant role in synaptic transmission by hydrolyzing the neurotransmitter ACh. The active site of AChE is a composite of the peripheral anionic site (PAS) rich in aromatic residues located at the gorge's entry on the enzyme's surface, and the active catalytic site (CAS) is located at the bottom of a 20 Å gorge.[14]

Intriguingly, the amount of AChE decreases in the course of AD. Whereas, the concentration of BChE remains unchanged or even increases, BChE can compensate for AChE loss, resulting in improved cognition.[15] In the AD brain, the level of BChE increases remarkably in the cortical region. Simultaneously, AChE activity decreases, and the ratio between BChE and AChE varies from 0.6 (normal brain) to as high as 11 (AD brain), which further leads to the development of neuritic plaques and neurofibrillary tangles, contributing to the severity of AD pathogenesis.[16] Interestingly, it has been shown in the literature that BChE inhibitors improve cognition by increasing ACh levels.[17,18] Therefore, dual-acting AChE/BChE inhibitors can be a practical therapeutic approach for effective and safe AD management.

AD brains have frequently shown the signature of reactive oxygen species (ROS) and reactive nitrogen species (RNS) mediated neuronal injury. An imbalance between ROS/RNS and the reduction in cells' capacity to neutralize these species creates a situation in the cells known as oxidative stress.[19,20] An increase in oxidative stress level is hypothesized to be one of the early events responsible for the disease's pathogenesis, which ultimately leads to neurodegeneration. Further, an imbalance in the mitochondrial redox system is associated with the generation of ROS. The reaction between the electrons leaked from the inner mitochondrial membrane and oxygen atom creates highly reactive superoxide anions ($O_2^{\cdot -}$). These superoxide radicals can further undergo free radical chain reaction to generate other ROS like hydrogen peroxide (H_2O_2) and hydroxyl ion (OH^-). Metals, especially copper and iron, also mediate oxidative stress.[21,22] The loss of antioxidant capacity of cells with age might also cause increased levels of oxidative stress. The overproduction of ROS and simultaneously increased level of antioxidant enzymes has been observed in the AD brain.[23] It is evident from recent publications that oxidative stress precedes the appearance of senile plaques and neurofibrillary tangles.[24,25] Therefore, the oxidative stress hypothesis has emerged as a crucial point for understanding the mechanisms leading to neurodegeneration and identifying novel neuroprotective therapies for AD. Consequently, antioxidants therapy for aging diseases has been of paramount importance in the last decade.[26–28] Antioxidant compounds curcumin and ferulic acid (**FA**) are known to reduce ROS and alleviate their toxic effects.

An increased level of metals, especially iron, and copper have been reported in the AD brain. Although metals are the utmost requirement for normal brain functioning, however, the imbalance in metal homeostasis can facilitate the overproduction of ROS and Aβ aggregation, which can create metal-induced oxidative stress (OS) in the brain.[29,30] In the presence of bio-metals like iron and copper ions, excessive production of hydrogen peroxide and $O_2^{\cdot -}$ can undergo Fenton reaction to create the highly reactive ($OH^{\cdot}$), resulting in neurodegeneration in AD. The increased level of metals also disrupts the redox system of the cell and further creates OS. The factors such as increased metals accumulation and decrease level of bodies' antioxidants such as glutathione peroxidase, lipid peroxidase can further contribute towards the increase in OS.[25] The different studies also suggested that OS is also responsible for the increased production of malondialdehyde (MDA) and 4-hydroxynonenal (4-HNE), which are the end products of lipid peroxidation.[31] Therefore, metal-induced toxicity and oxidative stress can interplay a crucial role in AD pathogenesis and progression.

The currently available pharmacotherapies for AD provide only symptomatic treatment without addressing aforesaid described the disease associated pathophysiological factors (Fig. 1). Consequently, the progression of the disease continues with the current therapies. At present, there is no cure for AD. Given the complex multifactorial nature of the disease, the identification of novel multifunctional therapeutic agents able to act on disease associated pathophysiological factors would be of great value to develop novel therapeutics. In our approach, along with this line, we designed compounds with both symptomatic and neuroprotective disease-modifying properties. Natural products such as **FA**, are the major sources of therapeutic agents for diseases, including neurodegenerative disorders (Fig. 1).[32] Given the significant role of **FA** *via* regulating oxidative stress in AD pathogenesis, **FA** is still not druggable and suffers from several shortcomings that limit its application as an anti-AD agent.[33] In our ongoing efforts to develop naturally inspired multifunctional therapeutics targeting, earlier we reported a series of AChE/BChE inhibitors based on **FA** template that possesses potential antioxidant, iron-chelation ability, and $A\beta_{1\text{-}42}$ aggregation modulation property.

To improve the cholinergic inhibition, and antioxidant property, we have further extended out the structure–activity relationship (SAR) studies of this series of molecules. Earlier, we have identified phenyl piperazine derivative (**PPD**, **EJMC-B**) exhibiting promising free radical quenching ability ($IC_{50} = 61.98 \pm 0.30$ μM) in 2,2-diphenyl-1-picrylhydrazyl (DPPH) assay with a potency comparable to that of parent natural compound **FA** ($IC_{50} = 56.49 \pm 0.62$ μM). Intriguingly, majority of the developed PPD's were devoid of potent ChEs activity. Therefore, the first series of novel molecules were designed, synthesized, and evaluated for AChE/BChE inhibitory property to investigate the effect of the replacement of phenylpiperazine ring with benzylpiperazine. Next, the linker length between **FA** and substituted phenyl ring was increased to explore the role of linker size on enzyme inhibition and selectivity. Finally, we also wanted to observe the effect of replacing the 5-aminoindole moiety in our earlier reported molecule **EJMC-G** (Fig. 2) with a tryptamine derivative on AChE/BChE activity. The structural modifications were carried out in a calibrated manner while maintaining the ClogP of the developed molecules in the desired range as per earlier our publications.[26] The selected compounds were evaluated for the enzyme kinetic, and PAS binding studies. Next, we carried out detailed computational studies to corroborate our *in-vitro* studies and gain an insight into the interactions between developed molecules and AChE/BChE using molecular docking and MD simulation studies. Further antioxidant potential and metal chelation studies were carried out. The evaluation of the effect of the treatment with different doses of the lead molecule on

reversing H_2O_2-induced toxicity in the neuronal N2a cells was carried out. The blood–brain barrier crossing ability of lead-developed molecules was examined in parallel artificial membrane permeability assay-blood brain barrier (PAMPA-BBB) assay. Finally, we evaluated the treatment effect with different doses (5 and 10 mg/kg) of **13b** in reversing the scopolamine-induced memory impairment in Morris water maze test.

2. Results and discussion

2.1. Chemistry

New ferulic acid-benzyl piperazine hybrids **3a-3p** were obtained as mentioned in Scheme 1. The synthesis of target compounds was completed using a well-established synthetic method. Commercially available benzyl halides (**1e-1g, 1i** and **1m-1o**) underwent nucleophilic substitution reaction (SN2) with piperazine in ethanol to give compounds **2e-2g, 2i,** and **2m-2o**. The target compounds **3a-3p** were obtained by the reaction of substituted benzylpiperazine (**2a-2p**) with **FA** using the standard amide coupling method 1-ethyl-3-(3-dimethylaminopropyl)carbodiimide hydrochloride (EDCI.HCl), hydroxybenzotriazole (HOBt), and N,*N*-diisopropylethylamine (DIPEA). The compound **3a** has been reported earlier in the literature as an intermediate for the development of **FA** based therapeutic agents for AD.[34] The molecular hybrids of **FA** and substituted amines connected with alanine linker were synthesized by following the reaction steps mentioned in Scheme 2. In the first step, *N*-Boc-propanamide derivatives (**6a-6c**) were obtained by standard amide coupling of substituted amines with Boc-alanine. In the next step, *N*-Boc-protected secondary amine groups were then deprotected by ether HCl to yield **7a-7c**. Finally, the compounds **8a-8c** were synthesized by the reaction of substituted alanine, **FA** using standard amide coupling. To obtain **FA**-tryptamine-based hybrid analogs (**13a-13c**), we followed the synthetic route depicted in Scheme 3. First, the Boc-glycine was reacted with a substituted tryptamine (**10a-10c**) to obtain the desired intermediates **11a-11c**. After Boc deprotection, the final compounds (**13a-13c**) were obtained using standard amide coupling with **FA**. All newly synthesized hybrids were purified by chromatographic techniques and structurally characterized by ^{1}H NMR, ^{13}C-NMR, and high-resolution mass spectrometry (HRMS, **Table S1**).

2.2. Design and cholinesterases inhibition studies of novel naturally inspired *FA* analogs

2.2.1. Design of novel naturally inspired *FA* analogs

In our continuous efforts to develop naturally inspired multifunctional molecules for AD management, earlier we reported a novel series of **FA** template-based AChE/BChE inhibitors that possess potential antioxidant, $A\beta_{1\text{-}42}$ aggregation modulation property, and iron-chelation ability.[26] One of the major goals behind the novel **FA** analogs' design is to improve the AChE inhibition, and antioxidant potential of **FA**-derived compounds. One of the findings from our previous SAR studies that we observe a loss in the free radical quenching ability of most developed molecules compared to **FA**. Intriguingly, the phenyl piperazine derivatives (**PPD**) **EJMC-A-C** (Fig. 2) have shown promising free radical quenching ability (IC_{50} = 61.98 ± 0.30 μM for **EJMC-B)** in DPPH assay with a potency comparable to that of parent natural compound **FA** (IC_{50} = 56.49 ± 0.62 μM). However, we have shown that the coupling of substituted phenyl piperazine moiety with **FA** with glycinamide linker leads to a mixed impact on AChE/BChE inhibition. The developed **PPD** were found to be moderate to weak inhibitors of the target enzymes (IC_{50}, AChE, 9.91 ± 0.07 to 29.34 ± 0.03 μM, % BChE inhibition, 26.89 ± 0.20 to 44.71 ± 0.05). Given the key role of OS in AD pathogenesis and the potent antioxidant potential of the developed **PPD**, we planned to improve upon the AChE/BChE while maintaining ClogP of the designed molecules in the desired range as per our earlier publication.[26] Based on our studies, we hypothesized that the nature of the long active site of AChE/BChE and the relatively short structure of **PPD** is probably the reason for their moderate inhibitory activity. Hence, in the first series of SAR studies, we planned to introduce a spacer between phenyl and piperazine ring in the designed molecules. Therefore, the phenylpiperazine ring was replaced with benzylpiperazine. Thus, compounds **3a-3p** were designed and synthesized to improve the AChE/BChE inhibition and antioxidant potential while maintaining ClogP in the desired range (Table 1). The addition of hydrophobic features will also help the analogs to be able to interact with the essential hydrophobic residues at the active site of the enzymes. Despite these structural modifications, none of the tested compounds showed a significantly improvement in the enzyme inhibition studies compared to the earlier reportedPPD. Therefore, to further improve upon the AChE/BChE inhibition, we planned to increase the linker length in our earlier reported potent cholinergic inhibitors glycine amide derivatives **EJMC-D, EJMC-E**, and **EJMC-F** (Fig. 2). In our earlier study, we have demonstrated that our **FA** derivatives exhibited highest potency when the methylene linker length is one (n = 1). In this manuscript, we rationally and selectively synthesized only three molecules (**8a-c**), as a part of our SAR study, with a linker length two to observe whether this structural modification can further potentiate cholinergic inhibitions. Therefore, to evaluate the effect of a two-methylene linker size connecting **FA** and phenyl ring, compounds **8a-c** were designed and synthesized (Scheme 2). Intriguingly, none of the developed compounds showed an improved AChE/BChE inhibitory property (Table 1) over the earlier reported compounds (**EJMC-D, EJMC-E**, and **EJMC-F)**. One of the major goals of this study is to improve upon the enzyme inhibition and antioxidant properties of our earlier identified molecules. In our recent publication, we have identified **EJMC-G** (Fig. 2) as a potential multifunctional agent able to provide both symptomatic relief and neuroprotection for the management of AD.

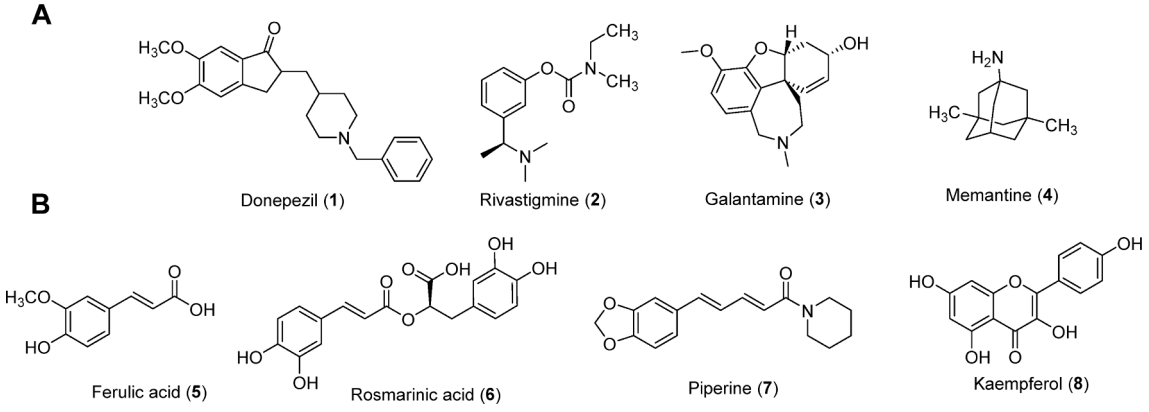

Fig. 1. Chemical structures of (**A**) Drugs available in the market for the treatment of AD. (**B**) Natural products known to modulate neurodegenerative disorders.

Given the significant role played by the presence of indole moiety in **EJMC-G** in the interaction with the target enzymes and antioxidant property, the 3rd series of compounds where **FA** and tryptamine moieties were joined through optimized glycine amide to improve upon the AChE/BChE inhibition and antioxidant property.

2.2.2. Cholinesterases inhibition studies

Given the significant role played by ACh and butyrylcholine (BCh) in memory and cognitive impairment in various stages of AD, therefore, cholinesterase's inhibitory activity of the newly synthesized compounds against human AChE and equine BChE was measured by using the spectroscopic method of Ellman *et al.*[35] The inhibitory activity is expressed as IC_{50}, *i.e.*, the inhibitor concentration that reduces the cholinesterase activity by 50%. In this study, **DPZ** served as the reference drug, and **FA** was used as the negative control.

In our initial attempt to explore the possible changes in enzyme inhibition properties due to such structural changes, compound **3a** was synthesized and evaluated for ChEs inhibitory activities. In the enzyme inhibition studies, **3a** bearing unsubstituted benzylpiperazine fragment exhibited potent AChE inhibitory property (IC_{50}, AChE (μM) = 13.34 ± 0.28) compared to **EJMC-A** (IC_{50}, AChE (μM), = 29.34 ± 0.03). Interestingly, **3a** (Fig. 2) was approximately twice more potent compared to (**EJMC-A**). However, in the BChE inhibition assay, **3a** turned out to be equipotent compared to **EJMC-A** (% BChE inhibition 45.13 ± 0.61, and 37.03 ± 0.41 for **3a** and **EJMC-A,** respectively**)**. This result indicated that benzylpiperazine fragment was well tolerated on the enzyme sites. Further, the methyl group was introduced on various positions of the phenyl ring of benzyl piperazine fragment, leading to the generation of compounds **3b-3d**. Intriguingly, compounds bearing methyl group at different position of benzylpiperazine fragment showed weak inhibition towards AChE over **3a** (IC_{50}, AChE (μM), >20 for **3b-3d**) over the earlier reported 4-methyl phenylpiperazine derivative **EJMC-C** (IC_{50}, AChE (μM) = 19.48 ± 0.12, **EJMC-C**, Fig. 2). Intriguingly, in case of BChE inhibition assay the developed molecules were found to be potent inhibitors over **3a** (IC_{50}, BChE (μM), **3b** = 15.06 ± 0.38, **3c** = 14.69 ± 0.35, and **3d** = 14.75 ± 0.31 μM, and % BChE inhibition 37.03 ± 0.41 for **3a**). It is worth mentioning that in the case of BChE inhibition, substitution of a methyl group on benzylpiperazine was better tolerated over our earlier reported methyl-substituted phenylpiperazine compound **EJMC-C** (% BChE inhibition 38.14 ± 0.12). To further validate our previous results on the electron donating group (EDG), we introduced monomethoxy group onto our parent molecule **3a,** which led to the generation of compounds **3e** (*o*-OCH_3), and **3f** (*p*-OCH_3). In the enzyme inhibition assay, the compounds with monomethoxy group effectively inhibited AChE and were equally potent to **3a** (IC_{50}, AChE (μM), **3e** = 15.18 ± 0.36, and **3f** = 16.39 ± 0.42). However, introduction of monomethoxy group on the benzylpiperazine a significant reduction towards BChE inhibition was observed compared to **3b-3d** (% BChE inhibition 49.12 ± 0.63 and 45.13 ± 0.67, **3e** and **3f,** respectively). These results concur with our previous finding with the **PPD** where we observed that the introduction of methoxy group could increase the developed molecules inhibitor activity towards AChE.

We further explored various electron-withdrawing groups (EWGs) on benzylpiperazine ring to explore the significance of various electronic features on the AChE/BChE inhibition. Therefore, compounds **3g-3l** were designed, synthesized and evaluated for the enzyme inhibition assays. In this study, **3k** bearing *m*-fluoro turned out to be most potent among all developed molecules so far [IC_{50}, AChE (μM), **3h** (*m*-chloro) = 15.43 ± 0.28, **3k** (*m*-fluoro) = 13.13 ± 0.26, and **3l** (*p*-fluoro) = 14.54 ± 0.65 μM]. Interestingly, all the developed molecules (**3g-3l)** were found to be equipotent inhibitors of BChE [IC_{50}, (μM), **3g** (*o*-chloro) = 15.21 ± 0.29, **3h** (*m*-chloro) = 14.80 ± 0.34, **3i** (*p*-chloro) = 15.86 ± 0.31, **3j** (*o*-fluoro) = 15.89 ± 0.23, **3k** (*m*-fluoro) = 14.03 ± 0.22, and **3l** (*p*-fluoro) = 14.85 ± 0.37 μM]. We further introduced bulky EWGs on the benzylpiperazine fragment in order to explore their effect on enzymes inhibition properties. Therefore, compound **3m-3p** were developed and evaluated for enzymes inhibition. Surprisingly, all developed compounds exhibited weak inhibitory activity towards AChE (IC_{50}, AChE (μM), >20 μM). In contrast, the developed molecules **3m-3p** were found to be potent inhibitors of BChE over **3a** (IC_{50}, BChE (μM), **3m** = 14.89 ± 0.26, **3n** = 14.73 ± 0.31, **3o** = 15.58 ± 0.44, and **3p** = 14.62 ± 0.16 μM, respectively).

Despite these promising results, none of the tested compounds showed a significantly improved enzymes inhibition studies than earlier reported phenylpiperazine derivatives. Therefore, to improve upon the AChE/BChE inhibition, compounds **8a-c** were designed and synthesized (Scheme 2). To evaluate the effect of a two-methylene linker size connecting **FA** and phenyl ring, compounds **8a** was designed and synthesized (Scheme 2). This compound exhibited slightly more potent activity towards AChE ($IC_{50,}$ AChE (μM) = 14.75 ± 0.42) while significant increase in BChE inhibition ($IC_{50,}$ BChE (μM) = 16.38 ± 0.37) was observed in comparison to **EJMC-F** [$IC_{50,}$ AChE (μM) = 21.94 ± 0.81, BChE (% inhibition) = 38.25 ± 0.25]. Our earlier enzyme inhibition studies also demonstrated that compounds with *m*-methoxy and *p*-chloro on the terminal phenyl ring are comparatively potent enzyme inhibitors over the other developed **FA** analogs. We specifically incorporated these groups in the development of molecules **8b-8c** with increased linker length to investigate the impact of linker length on the enzyme inhibition. Among the three compounds (**8a-8c**), **8b** exhibited maximum inhibition for AChE (IC_{50}, AChE (μM) = 2.41 ± 0.42). While **8c** was found to be most potent inhibitor towards BChE (IC_{50}, BChE (μM) = 7.13 ± 0.37 μM). Thus, it demonstrates that the optimal methylene linker size is one in a similarly substituted series of **FA** template. These results indicated that the introduction of propenamide linker instead of glycine amide did not improve upon the enzymes inhibitory property.

The indole moiety played a key role in the interaction with targets enzymes and could also reverse the loss in antioxidant property as reported in the case of **EJMC-G**, therefore, tryptamine ring was introduced

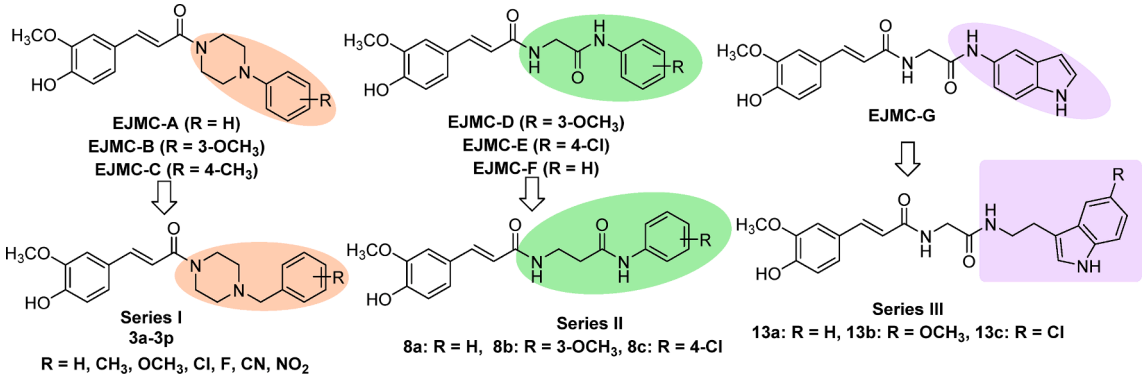

Fig. 2. Design of the multifunctional ChEs inhibitors by integrating the structural features of ferulic acid (**FA**) derivatives.

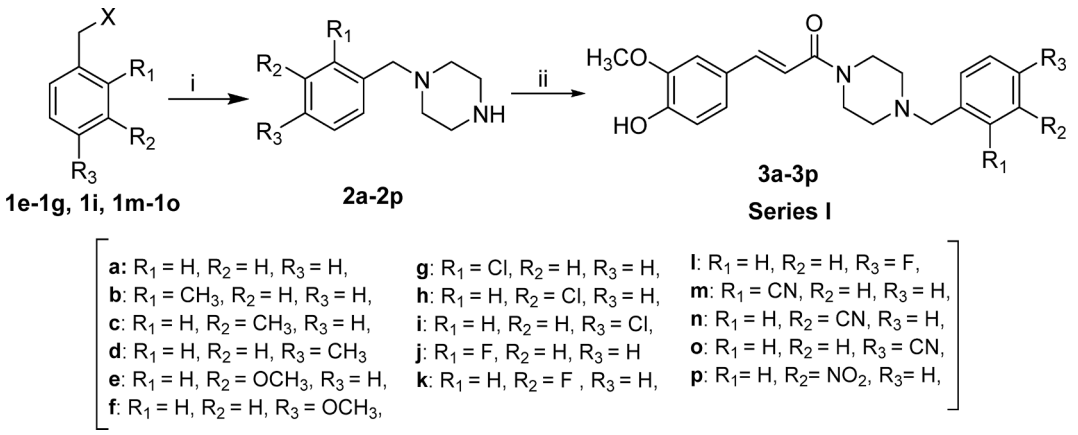

Scheme 1. Synthesis of compounds **3a-3p**. Reagents and conditions: (i) Anhydrous piperazine, K_2CO_3, ethanol, reflux, 4–5 h, 70–80%; (ii) **FA**, EDCI.HCl, HOBT, DIPEA, dry THF, rt, overnight, 65–75%.

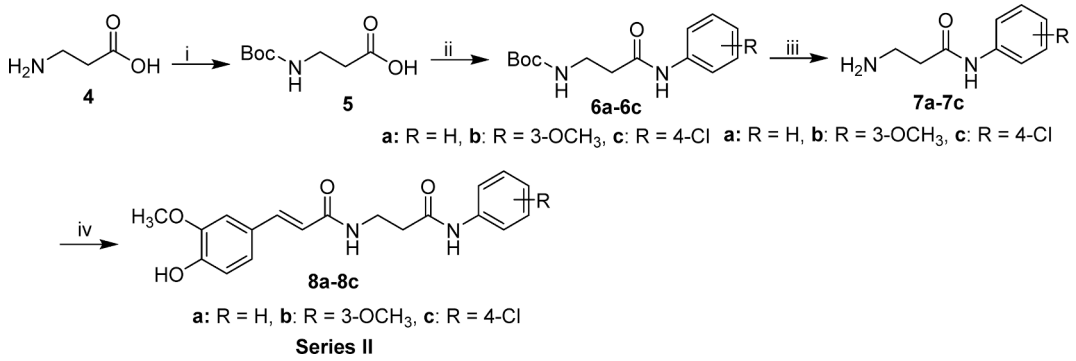

Scheme 2. Synthesis of designed compounds **8a-8c**. Reagents and conditions: (i) Boc-anhydride, DCM, 0 °C, overnight, 90%; (ii) aniline/3-methoxyaniline/4-chloroaniline, EDCI.HCl, HOBT, DIPEA, dry THF, rt, overnight, 70–75%; (iii) Ether HCl, methanol, rt, 12 h, 80–85%; (iv) **FA**, EDCI.HCl, HOBT, DIPEA, dry THF, rt, overnight, 70–75%.

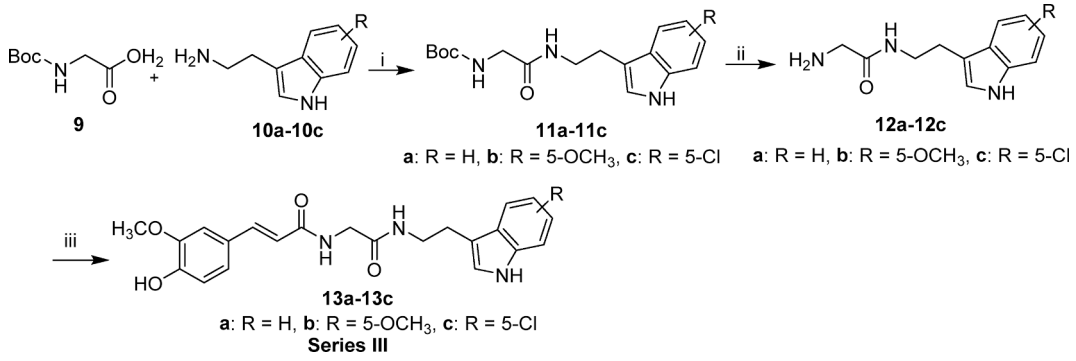

Scheme 3. Synthetic route to compounds **13a-13c**. Reagents and conditions: (i) EDCI.HCl, HOBT, DIPEA, dry THF, rt, overnight, 65–70%; (ii) Ether HCl, methanol, rt, 12 h, 80–85%; (iii) **FA**, EDCI.HCl, HOBT, DIPEA, dry THF, rt, overnight, 65–70%.

in the third series of molecules. In this series, three compounds were designed, synthesized, and evaluated for enzyme inhibition studies. Interestingly, compounds **13a-13c** bearing tryptamine functionality showed significant AChE/BChE inhibition over the earlier reported compounds. The developed molecules were found to be equipotent towards AChE inhibitory activity (IC_{50}, AChE (μM), **13a** = 1.42 ± 0.24, **13b** = 0.96 ± 0.14, and **13c** = 0.84 ± 0.12). Similarly, the developed compounds were found to be potent inhibitor of BChE (IC_{50}, BChE (μM), **13a** = 3.14 ± 0.28, **13b** = 1.23 ± 0.23, and **13c** = 1.29 ± 0.22). These results collectively suggested that both EWG or EDG on tryptamine moiety well tolerated on enzymes (SI, Fig. S1). The SAR on this series of all developed molecules is represented in Fig. 3.

2.3. Antioxidant activity (DPPH radical scavenging activity)

It is evident from the literature that OS plays a crucial role in the progression of AD. Therefore, inhibition of ChEs along with the ability to reduce OS would be a more effective approach for the treatment of AD. The antioxidant ability of developed molecules was evaluated by 2,2-Diphenyl-1-(2,4,6-trinitrophenyl) hydrazine (DPPH) assay. To perform DPPH radical scavenging experiment, we have selected 13 compounds based on ChEs inhibition property. Antioxidant activity is expressed as IC_{50} value, *i.e,* compound concentration required to reduce 50% of the DPPH radical concentration in a solution. All tested compounds exhibited excellent to moderate antioxidant activity with IC_{50} ranging

Table 1
Structures, ChEs inhibitory activities, cLogP, and tPSA of compounds **3a-3p**, **8a-8c** and **13a-13c**.

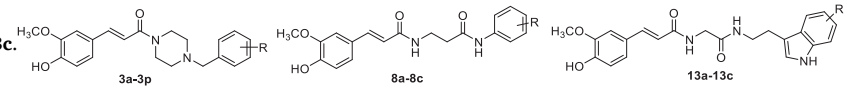

Compd.	R	IC_{50} (μM)[a] or % inhibition[b]		tPSA[c]	cLogP[c]
		*h*AChE	*eq*BChE		
3a	Hydrogen	13.34 ± 0.28	45.13 ± 0.61%	53.01	3.22
3b	2-methyl	43.10 ± 0.84%	15.06 ± 0.38	53.01	3.67
3c	3-methyl	45.50 ± 0.86%	14.69 ± 0.35	53.01	3.72
3d	4-methyl	43.16 ± 0.69%	14.75 ± 0.31	53.01	3.72
3e	3-methoxy	15.18 ± 0.36	49.12 ± 0.63%	62.24	3.14
3f	4-methoxy	16.39 ± 0.42	45.13 ± 0.67%	62.24	3.14
3g	2-chloro	46.99 ± 0.87%	15.21 ± 0.29	53.01	3.94
h	3-chloro	15.43 ± 0.28	14.80 ± 0.34	53.01	3.94
3i	4-chloro	37.26 ± 0.85%	15.86 ± 0.31	53.01	3.94
3j	2-fluoro	34.24 ± 0.78%	15.89 ± 0.23	53.01	3.37
3k	3-fluoro	13.13 ± 0.26	14.03 ± 0.22	53.01	3.37
3l	4-fluoro	14.54 ± 0.65	14.85 ± 0.37	53.01	3.37
3m	2-cyano	45.39 ± 0.67%	14.89 ± 0.26	76.8	2.80
3n	3-cyano	42.41 ± 0.51%	14.73 ± 0.31	76.8	2.66
3o	4-cyano	39.40 ± 0.78%	15.58 ± 0.44	76.8	2.66
3p	3-nitro	38.76 ± 0.52%	14.62 ± 0.16 104.82	104.82	2.97
8a	Hydrogen	14.75 ± 0.42	16.38 ± 0.37	87.66	2.26
8b	3-methoxy	2.41 ± 0.42	11.34 ± 0.46	96.89	2.34
8c	4-chloro	5.32 ± 0.31	7.13 ± 0.37	87.66	3.23
13a	Hydrogen	1.42 ± 0.24	3.14 ± 0.28	99.69	2.15
13b	5-methoxy	0.96 ± 0.14	1.23 ± 0.23 108.92	108.92	2.17
13c	5-chloro	0.84 ± 0.12	1.29 ± 0.22	99.69	3.03
FA[d]	–	15.12 ± 0.36%	17.15 ± 0.29%	66.76	1.42
DPZ[e]	–	0.06 ± 0.01	2.16 ± 0.19	38.77	4.59

[a] IC_{50}: 50% inhibitory concentration (mean ± SD of two or three independent experiments).
[b] % inhibition at 20 μM concentration of inhibitor.
[c] tPSA (topological polar surface area) and cLogP values are calculated using ChemDraw.
[d] **FA** (ferulic acid) = negative control.
[e] **DPZ** (donepezil) = reference standard.

from 20.25 ± 0.26 to 95.59 ± 0.57 μM (Table 2). Interestingly, compounds bearing *m*-fluoro (**3k**), and tryptamine (**13a**, **13b**, and **13c**) derivatives showed the maximum radical scavenging activity among all the tested molecules in this series (IC_{50}, **3k** = 26.58 ± 0.24, **13a** = 29.05 ± 0.32, **13b** = 20.25 ± 0.26, and **13c** = 23.57 ± 0.29 μM, respectively) (Fig. 4). The proposed mechanism of **13b** as a radical scavenger is shown in **Fig. S2**. Overall, our study suggests a significant improvement in the antioxidant property in the some of the newly developed molecules compared to earlier reported phenylpiperazine derivatives (**EJMC-B**, IC_{50} = 61.98 ± 0.30 μM), and the parent molecules **FA** (IC_{50} = 58.31 ± 0.61).

2.4. Kinetic studies of ChEs inhibition

The mechanism of ChEs inhibition (AChE & BChE) was evaluated for two selected lead compounds (**3k** and **13b**) on both human AChE (*h*AChE) and *equine* BChE (*eq*BChE). In this experiment, reciprocal of the substrate [S] *vs* reciprocal of velocity [V] curves were plotted upon addition of different concentrations of **3k** (26, 13, and 6.5 μM), and **13b** (5.0, 1.0 and 0.5 μM) in the presence of five different substrate [S] concentrations (ATCI or BTCI) (0.5, 1.0, 1.5, 2.0 and 2.5 μM for *h*AChE, and 5, 10, 15, 20, and 25 μM for *eq*BChE) to probe into the mechanism of ChEs inhibition. As depicted in Fig. 5 by Lineweaver–Burk reciprocal plots, **3k** and **13b** displayed a mixed type of inhibition on both *h*AChE and *eq*BChE (Fig. 5).

2.5. Peripheral anionic site (PAS) binding study

Based on the potent cholinergic inhibitory (IC_{50}, **3k** = 13.13 ± 0.26, **13b** = 0.96 ± 0.14, and **13c** = 0.84 ± 0.12 μM, respectively) and antioxidant properties (IC_{50}, **3k** = 26.58 ± 0.24, **13b** = 20.25 ± 0.26, **13c** = 23.57 ± 0.29, respectively) the lead molecules les **3k**, **13b**, and **13c** were selected for PAS binding studies. Next, to determine whether **3k, 13b,** and **13c** have an affinity towards the PAS of AChE, a propidium iodide-based competitive displacement assay was performed following our publications.[26] Propidium iodide is a commonly used PAS-specific ligand of AChE, which binds selectively at its PAS, which can be measured through the enhancement of the fluorescence intensity (~10-fold). In the presence of a ligand able to bind with strongly bind with PAS site, a decrease in the propidium iodide fluorescence is expected due to displacement of propidium from the PAS. DPZ, which is known to bind to the enzyme's PAS site, served as a reference drug in this assay. To perform this experiment, we incubated AChE (5.0 U/mL) with different concentrations of compounds (5, 10, 20, and 50 μM) followed by propidium iodide and recorded the change in fluorescence using Synergy™ HT, Bio-Tek Instruments, Inc. The results mentioned in Table 3 indicated that **13b** and **13c** were found to be more efficient to displace propidium iodide in a concentration-dependent manner compared to **DPZ**. While, **3k** represented weak propidium iodide displacement compared to **DPZ** and other tested compounds.

2.6. Molecular modeling studies

2.6.1. Molecular docking

Molecular docking of selected ligands **3a**, **3c**, **3g-h**, **3j-k**, **3m**, **8a**, **8c**, and **13b-c** were performed against the AChE and BChE using the Glide in extra precision (XP) mode. Before performing the final docking study of all above mentioned molecules, the co-crystallized ligands *i.e.* **DPZ** and Tacrine were redocked to the crystal structures of AChE and BChE, respectively. The RMSD difference between the redocked and co-crystallized ligands were found to be less than 1 Å. The **Tables S2 and S3** depicts the Docking score, XP GScore, glide gscore, glide emodel, and

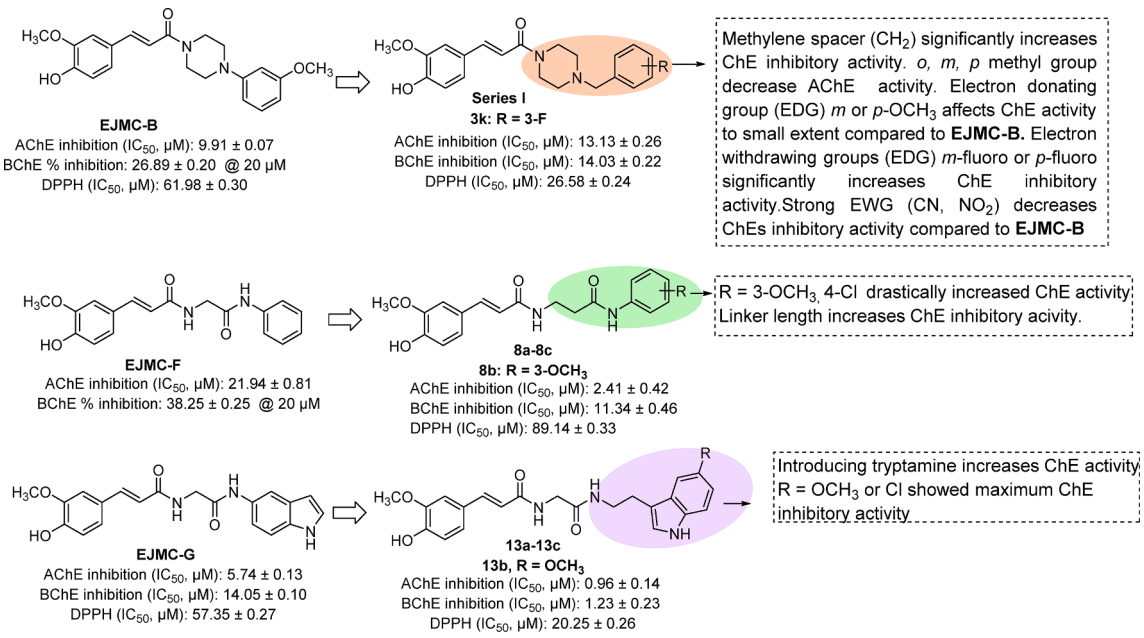

Fig. 3. Brief summary of structural activity relationship (SAR).

Table 2
Antioxidant activity (DPPH assay) of **3a**, **3c**, **3f**, **3h**, **3i**, **3k-3l**, **8a-8c**, **13a-13c** and **FA**.

Compound	DPPH assay	
	% Radical scavenging [a]	IC_{50} (μM) [b]
3a	38.41 ± 1.09	31.34 ± 0.45
3c	26.32 ± 1.13	65.98 ± 0.39
3f	30.49 ± 1.13	46.43 ± 0.29
3h	23.13 ± 1.17	61.52 ± 0.42
3i	32.41 ± 0.92	62.40 ± 0.45
3k	40.23 ± 1.21	26.58 ± 0.24
3l	23.14 ± 0.98	51.93 ± 0.41
8a	10.62 ± 0.96	95.59 ± 0.57
8b	21.28 ± 1.01	89.43 ± 0.46
8c	18.66 ± 0.96	84.21 ± 0.66
13a	38.55 ± 0.92	29.05 ± 0.32
13b	51.92 ± 1.12	20.25 ± 0.26
13c	47.27 ± 1.11	23.57 ± 0.29
FA[c]	33.11 ± 1.30	58.31 ± 0.61

[a] All the values were obtained at a compound concentration of 20 μM, % Radical scavenging; means ± SD of three independent experiments.
[b] IC_{50}: 50% inhibitory concentration (means ± SD of three independent experiments).
[c] **FA** (ferulic acid) = negative control.

important interactions (hydrogen bonds, hydrophobic interactions, and salt bridges) between residues of proteins (*i.e.* AChE and BChE) and small molecules.

2.6.2. *Interaction of ligands **3k** and **13b** with hAChE*

The Fig. 6A-B shows the 2D interaction diagram of **3k** and **13b** with *h*AChE. During the MD simulations it was observed that phenyl ring of **FA** moiety of ligand **3k** interacts with Trp286 *via* π- π stacking interaction, and this residue is considered as one of the principal components of PAS. This hydrophobic interaction between the Trp286 and **3k** was consistent and maintained during the entire simulation run as shown in protein–ligand contact histogram and timeline (**Figs. S3 and S4**). Similarly, the carbonyl moiety of **FA** exhibited water mediated hydrogen bond with Asp74 (PAS residue) and Thr75. In short, the whole **FA** fragment present in the ligand **3k** mainly interacts with residues belonging to PAS of AChE *via* hydrophobic and hydrogen bond interactions. Similarly, the piperazine ring of **3k** interacts with one of the important CAS residue Tyr337 via both direct and water mediated hydrogen bonds. This stable interaction of piperazine ring with CAS was maintained during the whole period of simulation *via* the water bridges and direct hydrogen bond (**Figs. S3 and S4**). Apart from this, one more important interaction between the 3-fluorobenzylpiperazine fragment and CAS residue Trp86 was observed which was maintained for 74% of total simulation time. Further, the residue Tyr341 makes π-cation interaction while the Phe 338 makes π- π stacking with the 3-Fluorobenzylpiperazine moiety, respectively.

The ligand **13b** is mainly composed of 3 moieties *i.e.* 5-methoxytryptamine, **FA** and a linker glycinamide (Fig. 6**B**). The 5-methoxytryptamine moiety of ligand **13b** mainly interacts with three CAS residues Trp86 (π-π stacking), Glu202 and Tyr337 (via water mediated hydrogen bond). The protein–ligand contact timeline representation depict that all of these interactions *i.e.* hydrogen bond and hydrophobic interactions between the tryptamine moiety and CAS residues were maintained throughout the simulation (**Figs. S3 and S4**). Further, a stable and consistent water mediated hydrogen bond between the 5-Methoxytryptamine of **13b** and Ser125 was also observed. One important and interesting interaction (hydrogen bond) between the carbonyl oxygen of **FA** moiety and residue Phe295 was also observed. Further, the protein–ligand contact histogram and timeline (**Figs. S3 and S4**) depicts that the interaction between Phe295 and **FA** moiety was one of the most consistent and stable interactions, since it was maintained for 99% of total simulation time.

2.6.3. *Interaction of ligands **3k** and **13b** to hBChE*

The Fig. 6C-D shows the 2D interaction diagram of **3k** and **13b** with *h*BChE. The **FA** moiety interacts with residues Tyr128, Gly115 via hydrogen bond, and Trp82 interacts via π- π stacking interaction. Further, the π-π stacking interaction between the fluorobenzyl moiety of **3k** and Phe329 was also observed.

The tryptamine moiety of **13b** makes a stable hydrogen bond with Ser287, and this interaction was maintained for 90% of total simulation time. Similarly, the **FA** moiety of the makes a couple of hydrogen bonds with residues Gly115 and Tyr128. The protein–ligand contact histogram and timeline (**Figs. S5 and S6**) shows that the interaction between the **FA** moiety of **13b** and Tyr128 was found to be stable and maintained

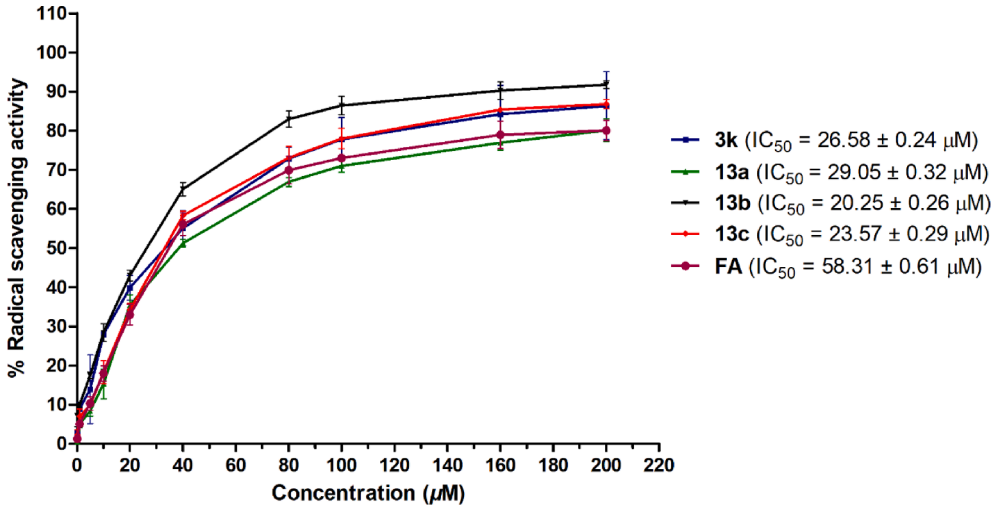

Fig. 4. DPPH scavenging activity by **3k**, **13a**, **13b**, **13c** and **FA**. Results are the means ± SD for the three-experiment performed in triplicate.

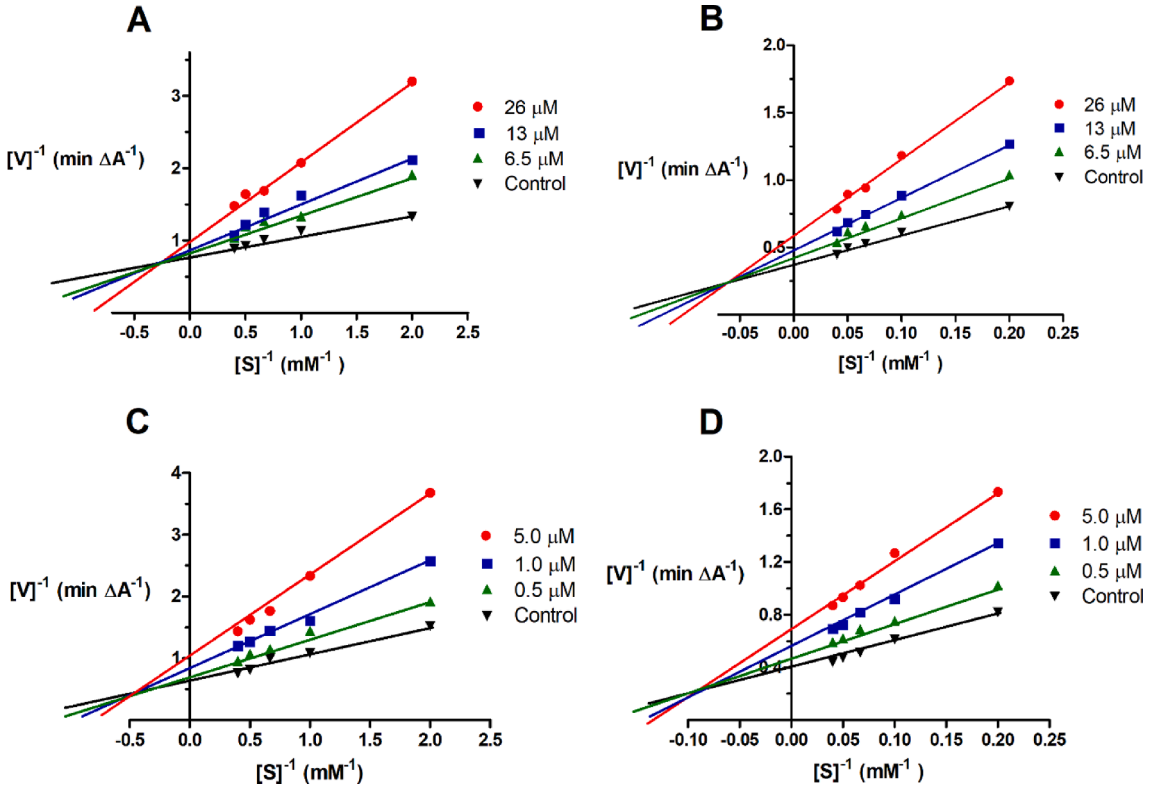

Fig. 5. Lineweaver-Burk double reciprocal plot showing the mechanism of *h*AChE and *eq*BChE inhibition over a range of substrate concentrations; [**A**, **B**] *h*AChE and *eq*BChE inhibition by **3k**; [**C**, **D**] *h*AChE and *eq*BChE inhibition by **13b**. The experimental data are the means ± SD of two independent experiments.

Table 3
Displacement of propidium iodide from the peripheral anionic site of AChE by **3k**, **13b**, **13c,** and **DPZ** at the indicated concentrations.

Code	5 μM	10 μM	20 μM	50 μM
3k	3.34 ± 0.12	8.32 ± 0.16	14.83 ± 0.24	20.32 ± 0.31
13b	10.36 ± 0.23	13.96 ± 0.29	21.85 ± 0.39	33.14 ± 0.43
13c	8.39 ± 0.26	13.64 ± 0.32	19.79 ± 0.42	30.17 ± 0.45
DPZ	8.87 ± 0.18	11.65 ± 0.22	19.10 ± 0.34	27.96 ± 0.41

[a]Results are the mean ± SD for two independent experiments.

during the entire simulation run. Apart from these interactions, the linker present between tryptamine and **FA** makes two hydrogen bonds with Thr120, and one water mediated hydrogen bond with Asn68.

2.6.4. *Analysis of binding free energy*

The binding free energy of complexes AChE_**3k**, AChE_**13b**, BChE_**3k** and BChE_**13b** were calculated from last 25 ns of trajectory at an interval of 50 ps using Prime/MM-GBSA (molecular mechanics/generalized born surface area) method. The Fig. 7 shows the fluctuation in binding free energy of all four complexes with respect to simulation time. Table 4 shows the average binding free energy and its different contributing terms for all four complexes. The Fig. 7A shows that the binding free

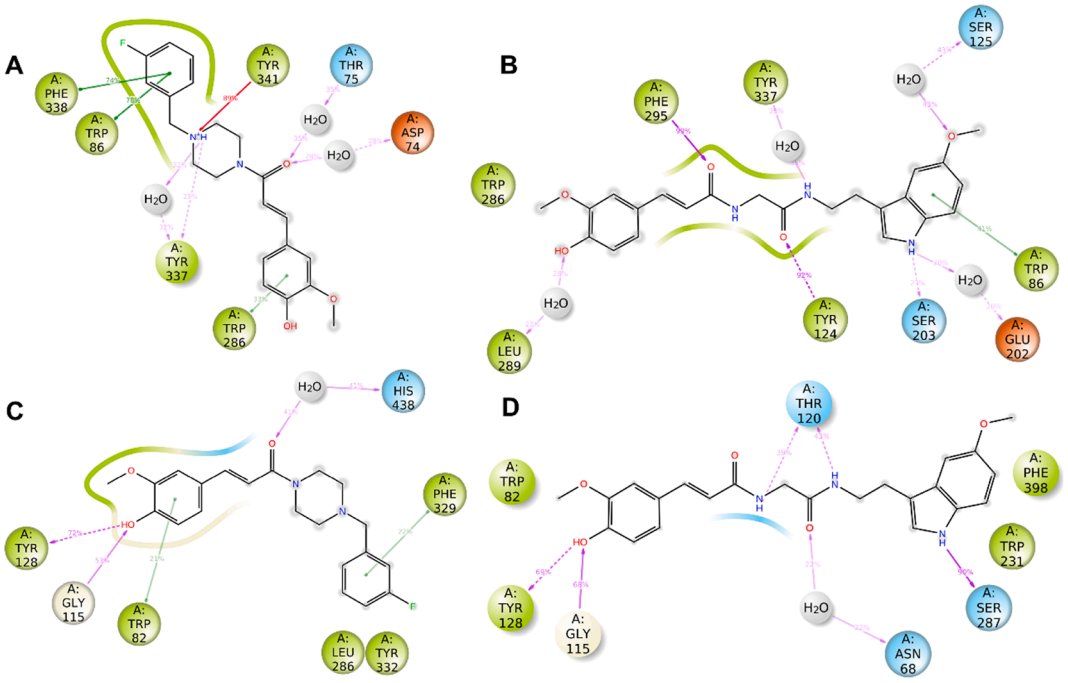

Fig. 6. 2D interaction diagram of (**A**) **3k** with AChE; (**B**) **13b** with AChE, (**C**) **3k** with BChE, and (**D**) **13b** with BChE. Whereas green, red and violet colored arrows represent the π-π stacking, π-cation interactions and hydrogen bonds, respectively.

energy of complex *h*AChE_**13b** fluctuates at higher values as compared to *h*AChE_**3k**. The average binding free energy of *h*AChE_**3k** complex in the last 25 ns was found to be −58.46 kcal/mol while the complex *h*AChE_**13b** was found to have −82.17 kcal/mol.

Similarly, the BChE_**13b** complex was found to fluctuate with higher binding free energy as compared to BChE_**3k** complex (Fig. 7**B**). The average binding free energy of BChE_**3k** complex was found to be −61.63 kcal/mol while BChE_**13b** complex has higher binding energy −75.03 kcal/mol. The calculated binding free energy for both ligand **3k** and **13b** with AChE and BChE are in line with observed experimental results.

2.6.5. Analysis of structural stability, compactness and solvent accessbility surface area

The structural stability of AChE and BChE and its complex with different ligands can be explained by analyzing the RMSD and radius of gyration (Rg) (**Figs. S7 and S8**). The changes in RMSD values with respect to simulation time for all complexes (AChE/BChE) suggest that the simulation is converged. It was observed that the RMSD fluctuates at lower values in presence of almost all ligands with respect to simulation time for both AChE and BChE (**Fig. S7**). This indicates that the binding of ligands stabilizes the AChE/BChE. The decrease in RMSD and Rg values of AChE with respect to simulation time in presence of ligands **3k**, **13b**, and **DPZ** are more significant as compared to BChE. There is very little or no considerable changes in Rg value of BChE in presence of all four ligands as compared to apo form of the enzyme (**Fig. S8**).

The percentage change in SASA of the residues presents 20 Å away from the binding pocket were also calculated for both AChE and BChE in the presence and absence of ligands. It was found that there was a considerable decrease in SASA of active site residues of both AChE and BChE in the presence of **3k** and **13b**. The **Fig. S9 A-B** represents the percentage decrease in SASA of AChE and BChE in the presence of **3k**, **13b** and crystallized ligands (**DPZ** and Tacrine) with respect to simulation time. The overall analysis shows that there was an average 6% decrease in SASA values of AChE in the presence of **3k**, **13b** and **DPZ**. Similarly, an average of around 5% decrease in SASA value was observed for BChE in presence of **3k**, **13b** and **DPZ**, while it was only

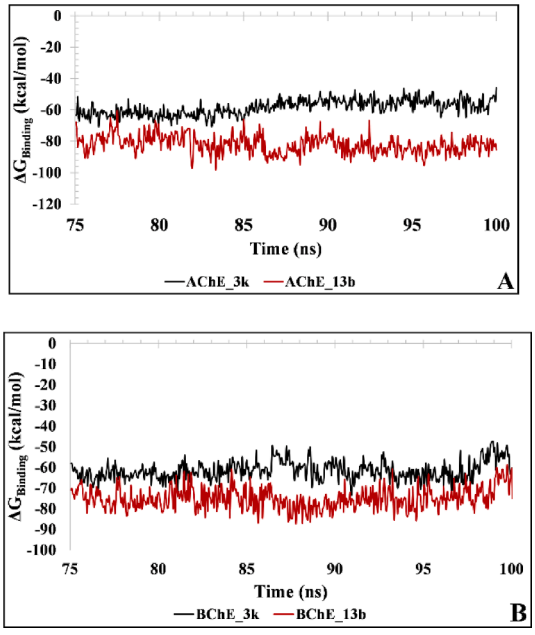

Fig. 7. Binding free energy of (**A**) AChE with ligands **3k** and **13b,** and (**B**) BChE with ligands **3k** and **13b**, with respect to simulation time calculated using the MM-GBSA method from the last 25 ns of MD simulations.

3.45% decrease in presence of co-crystallized ligand tacrine (**Fig. S9** (**B**), **Fig. S10A-C**).

2.7. Calculation of physicochemical parameters

Physicochemical properties such as molecular weight (MW), number of hydrogen acceptors (HBA), number of hydrogen donors (HBD), number of rotatable bonds (RB) and logBB were estimated using admetSAR software.[36] The values obtained were in range with the reported limits of CNS + drugs (SI, **Table S4**). Overall, these results

Table 4
The average ΔG_{bind} (Kcal/mol) and its different contributing energy terms for **3k** and **13b** against *h*AChE and *h*BChE calculated from MD trajectories (last 25) ns.

Complex	Avg. ΔG_{bind} Coulomb[a]	Avg. ΔG_{bind} Covalent[b]	Avg. ΔG_{bind} Hbond[c]	Avg. ΔG_{bind} Lipo[d]	Avg. ΔG_{bind} Packing[e]	Avg. ΔG_{bind} solv GB[f]	Avg. ΔG_{bind} vdW[g]	ΔG_{bind} Total[h]
AChE_**3k**	−22.50	1.81	−0.27	−27.69	−3.78	42.70	−48.73	−58.46
AChE_**13b**	−29.76	1.11	−1.44	−31.27	−7.39	46.70	−60.12	−82.17
BChE_**3k**	−12.35	2.81	−1.10	−31.02	−3.15	33.17	−50.01	−61.63
BChE_**13b**	−27.70	6.48	−2.21	−26.81	−2.02	38.12	−60.89	−75.03

[a] Coulomb energy.
[b] Covalent binding energy.
[c] Hydrogen bonding correction.
[d] Lipophilic energy.
[e] *Pi*-pi packing correction.
[f] Generalized Born electrostatic solvation energy.
[g] Van der Waals energy.
[h] Total binding free energy.

collectively suggests that all the developed compounds follow Lipinski's rule and exhibited significant brain permeability.

2.8. Metal chelation study

Literature studies revealed that the dyshomeostasis of biometals, especially iron (Fe) and copper (Cu), plays a crucial role in AD's pathogenesis. The extracellular accumulation of bio-metals induces the OS and leads to the generation of highly toxic reactive free radical species. Therefore, AD treatment through modulation of these bio-metals has been considered a viable therapeutic approach. Therefore, based on the AChE/BChE inhibition and antioxidant property, **13b** was selected for the iron-chelating ability. The metal chelating ability of representative compound **13b** was performed by UV–vis spectroscopy assay, and the results are presented in the Fig. 8. To perform this experiment, equimolar concentration of **13b** and $FeCl_3{\cdot}6H_2O$ were mixed together, and a complexation study was conducted (**Fig. S11**). As depicted in Fig. 8**, 13b** in the presence of $FeCl_3{\cdot}6H_2O$ presented different absorption spectra compared to absorption of the compound **13b** alone. The absorption spectra of the solution at pH 7.4 exhibited higher intensity at 511 nm than the spectra at lower pH values (4.2) (Fig. 8**)**. This is the clear indication of a complex formation between **13b** and Fe^{3+} ion. The binding stoichiometry of **13b** with Fe^{3+} was examined by measuring the changes in absorption at 511 nm when **13b** was titrated with $FeCl_3{\cdot}6H_2O$ in a different molar ratio, as depicted in fig. 8**C.** Finally, we plotted the absorbance value against the mole fraction of **13b.** We observed that there is a breakage point in the plot where the mole fraction of **13b** was 50%, which reveals 1:1 binding of **13b** toward Fe^{3+}(Fig. 8**D,** **Fig. S12**).

2.9. In-vitro evaluation of cytotoxicity of compound *13b*

The cytotoxicity studies are one of the important criteria in the drug development process. The cytotoxicity studies were carried out prior the *in-vivo* studies. The lead identified molecule **13b** with potent AChE/BChE inhibitory activity, antioxidant, and metal chelation properties was selected to evaluate the potential for cytotoxic effect on N2a cells, a widely used neuronal cell line. The cells were treated with different

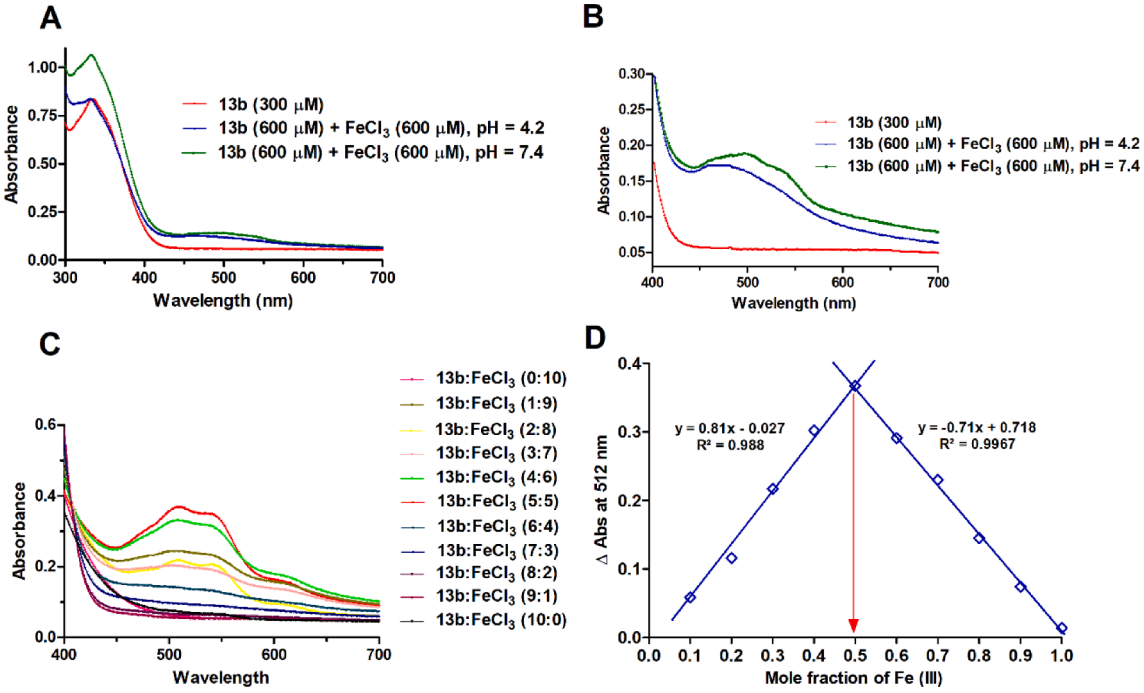

Fig. 8. (**A**) UV absorbance spectra of **13b** (300 μM) alone or in the presence of $FeCl_3$ (600 μM) in methanol (pH 4.2 and 7.4) from 300 to 700 nM. (**B**) UV absorbance spectra of **13b** (300 μM) alone or in the presence of $FeCl_3$ (1:1 equiv.) in methanol (pH 4.2 and 7.4) from 400 to 700 nm (*dd*-transition). (**C**) Metal ion titration of **13b** with $FeCl_3$ in different molar ratio (0–10 ratio). (**D**) Job's plot for determining the stoichiometry of the complex between **13b** and $FeCl_3$. Results are the means for the experiment performed in duplicate.

concentrations of **13b** for 24 hrs, and cell death was quantitatively analyzed by 3-(4,5-dimethylthiazol-2-yl)-2,5-diphenyltetrazolium bromide (MTT) assay. The dose-dependent effect of **13b** (Fig. 9**)** on cell viability indicated that the compound had no significant effect on cell viability and well tolerated by neuronal cells at all the tested concentrations.

2.10. Neuroprotective effect on H_2O_2 induced SH-SY5Y cell injury

In our previous experiment, **13b** has shown promising free radical quenching ability in 2,2-diphenyl-1-picrylhydrazyl (DPPH) assay, which strongly suggested that **13b** is a potent antioxidant with a potency approximate three times (IC_{50} = 20.25 ± 0.26 μM) compared to parent natural compound **FA** (IC_{50} = 58.18 ± 0.52 μM). In our present study, we carried out experiments to evaluate the effect of treatment with **13b** on protecting the neuronal N2a cells from toxicity induced by H_2O_2. In this experiment, we have employed various concentrations (100 to 800 μM) of the pro-oxidant H_2O_2 (widely acceptable neurotoxin) and found that 600 μM of H_2O_2 can cause ~50% cell death in N2a cells (Fig. 10**A**). After optimizing the concentration of H_2O_2 and the incubation time, we next assessed the neuroprotection ability of **13b**, to alter cytotoxicity after co-incubating with H_2O_2. The cells were incubated with various concentrations (1, 2.5, 5, 10, and 20 μM) of **13b** for 24 h followed by co-treatment with 600 μM H_2O_2 for an additional 24 h. As shown in fig.10**B** the MTT assay indicated that **13b** could significantly (*$P < 0.05$, ***$P < 0.001$) protect N2a cells from H_2O_2 induced neurotoxicity. The significant protection conferred by **13b** was exhibited in all tested concentration ranges of 1–20 μM of the drugs. However, no significant difference was observed at concentration above 2.5 μM. This suggest that 2.5 μM of **13b** is able to negate the oxidative stress caused by 600 μM of H_2O_2 in cells.

2.11. In-vitro blood–brain barrier permeation assay

Blood-brain barrier (BBB) permeability is the necessary requirement for developing anti-AD drugs. A parallel artificial membrane permeation assay of the blood–brain barrier (PAMPA-BBB) was performed to check the probable BBB permeability of **3k** and **13b**. For this experiment, firstly, we compared three commercial drugs' permeability with their reported values to validate the experiment (Table 5). The P_e values of **3k** and **13b** are listed in Table 5. According to the limit established by Di *et al.* for BBB permeation, we concluded that compounds with $P_e > 4.0$ could be considered to show high BBB permeability (CNS+), compounds with $P_e < 2$ is expected to show low BBB permeability (CNS-). Analysis of the developed compounds in the PAMPA-BBB assay revealed $P_e > 4.0$ for **3k,** and **13b** showed (Table 5), demonstrating that compound ability to cross the BBB and can potentially reach their biological targets within the brain.

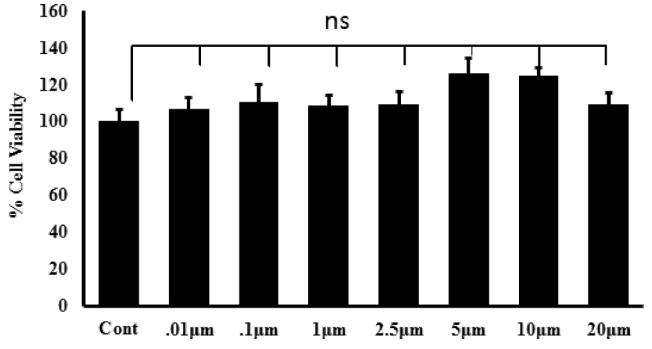

Fig. 9. Effect of **13b** on cell viability. Cells were treated with different concentrations of **13b** (0.01, 0.1, 1, 2.5, 5, 10 and 20 μM) for 24 h. Cell viability in % was analyzed using MTT assay. Data represented as mean ± SE of three independent experiments done in three replicates.

2.12. *13b* ameliorates scopolamine-induced cognitive impairment in the Morris water maze test

The improvement in cognitive impairment is the essential criteria for the successful development of anti-AD agents. The MWM permits the accurate and reproducible study of reference memory, cognitive maps, place learning, spatial learning, and working memory.[38,39] MWM is highly sensitive in the assessment of damage to the hippocampus. The robustness and reliability make this paradigm as one of the "gold standards" of behavioral neuroscience. Therefore, in the present study, we evaluated the *in-vivo* efficacy of **13b** in MWM experiment to assess the spatial working memory in mice (Fig. 11 A-B) . The respective drug doses of **13b** (5 and 10 mg/kg) orally, and **DPZ** (0.5 mg/kg) were administered intraperitoneally 30 min prior to the administration of scopolamine (1 mg/kg, *i.p.*) to the respective group of animals for consecutively fourteen days. During the last 5 days of the treatment period, ELTs were recorded for the animals of different experimental groups. The escape latencies time and the track diagrams for the first four days of the training period are shown in the **Figs. S13 and S14**. Scopolamine treatment caused a cognitive impairment and an increase in the escape latency time compared to the control group was observed which indicated the development of amnesia in the mice (Fig. 12A). While **DPZ** significantly reduced ELT from 33.58 ± 3.54 to 16.37 ± 5.11 s, $p < 0.01$, **Figs. S13** and **12A**) as compared to the scopolamine-treated group. Treatment with **13b** at dose of 10 mg/kg significantly reduced ELT from 50.11 ± 5.91 to 32.28 ± 6.37 s (**Fig. S13 & 12A**, $p< 0.05$) which indicates significant attenuation in the memory impairment. Additionally, the recorded tracks of the mice from all groups clearly further confirmed these results (Fig. 12C). These outcomes collectively suggested that the animals could retained the previous memory in the MWM experiment. The mechanism of the spontaneous alternation stimulation in the scopolamine model is likely mediated by the anti-AChE activity of the compound **13b**, suggesting that **13b** is a potent cholinesterase inhibitor that can cross the blood–brain barrier effectively. The results suggested that molecule is orally active and significant changes in the compound treated group in comparison with the control and the scopolamine group.

3. Conclusion

In this paper, we have further extended the SAR studies on our earlier identified FA template based novel series of molecules by using various strategies with the aim of finely tuning the ChEs inhibition activities and antioxidant property. All synthesized compounds were tested for their AChE and BChE inhibitory properties. The *in-vitro* enzyme inhibition studies suggested that the presence of tryptamine moiety could significantly improve the inhibitory activities of these molecules towards the AChE and the BChE. Several compounds from this developed latest series, for example, **8a-8c**, and **13a-13c**, can be considered as dual acting cholinestrases inhibitors because they were turned out to be effective inhibitors of the both the enzymes and able to interact with the key amino acid residues responsible for hydrolysis of cholinestrases. Compound **13b-13c** exhibited the highest activity for the AChE/BChE in the current series. The enzyme kinetic studies demonstrated a mixed type of inhibitory nature of **3k** and **13b** on both the AChE and BChE. The lead molecules **3k** and **13b** also exhibited significant antioxidant activity in the DPPH assay. Interestingly, **13b** was found to be three times more potent antioxidant in a DPPH assay (IC_{50} = 20.25 ± 0.26 μM) over the earlier identified **EJMC-B** (IC_{50} 61.98 ± 0.30) and it also was able to chelate iron. The PAMPA-BBB assay demonstrated that **3k**, and **13b** and could effectively cross BBB and can reach to their target located in the brain. The results from cell-based cytotoxicity studies indicated that the compound had no significant effect on cell viability at all the tested concentrations. Further, in *in-vitro* assays, **13b** exhibited neuroprotection property against H_2O_2 induced neurotoxicity in N2a cells and able to reverse the toxicity induced through OS. Compound **13b**

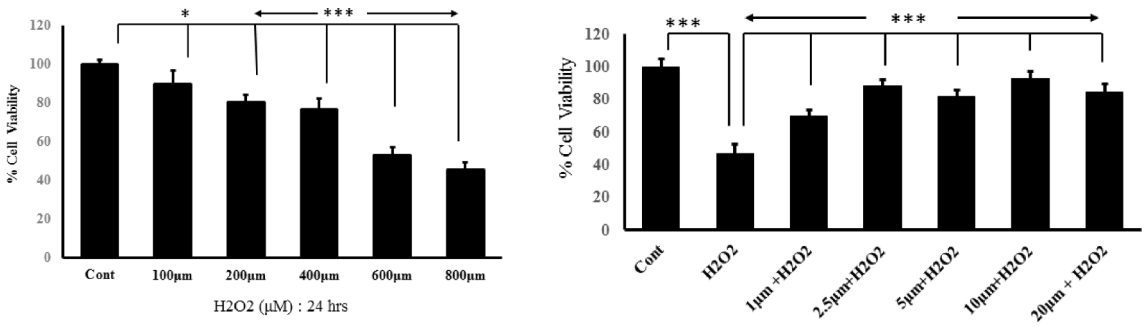

Fig. 10. Effect of **13b** against H_2O_2 mediated cell death. (**A**) Cell death induced by H_2O_2 at 100, 200, 400, 600, and 800 µM for 24 h. (**B**) Neuroprotective effect of treatment **13b** against H_2O_2 mediated N2a cell death. Cells were pre-incubated with **13b** at 1, 2.5, 5, 10, or 20 µM for 24 h and then further co-incubated with 600 µM H_2O_2 for another 24 h. Cell death was assessed by MTT assay. The data represent the mean of three independent experiments. *P < 0.05, ***P < 0.001, compared with untreated control cells only, data expressed as mean ± SEM.

Table 5
Permeability ($P_e = 10^{-6}$ cm s^{-1})[a] in the PAMPA-BBB assay for **3k**, **13b**, **DPZ**, testosterone, corticosterone, and hydrocortisone with their predictive BBB penetration.

S.No.	compound	P_e (exp)[a]	Reference value[b]	Prediction[c]
1.	Testosterone	18.91 ± 1.42	17.0	CNS (+)
2.	Corticosterone	10.19 ± 1.39	5.1	CNS (+)
3.	Hydrocortisone	2.94 ± 1.12	1.9	CNS (-)
4.	**3k**	9.57 ± 0.27	–	CNS (+)
5.	**13b**	8.51 ± 0.31	–	CNS (+)
6.	**DPZ**	15.57 ± 0.18	–	CNS (+)

[a] Data are the mean ± SD of two independent experiments.
[b] Reference values were taken from Di Li *et al.*[37].
[c] CNS (+), $P_e > 4.0$, high permeability; CNS (-), Pe < 2.0, low permeability; CNS (±), $4.0 > P_e > 2.0$, uncertain permeability. [d]DPZ (donepezil) reference AChE inhibitor. The data represent the mean ± SD of two independent experiments.

exhibited promising *in-vivo* activity in the scopolamine-induced in MWM model. . These above results confirm that **13b** is orally active and could be a lead candidate for further development of potential AD therapeutics. To uncover the full potential of the molecule further mechanistic studies will be carried out in detail in AD models.

4. Experimental section

4.1. Chemistry

All the solvents required for the synthesis of the compounds were dried by solvent distillation techniques before use. All the chemicals and reagents were obtained from the Sigma-Aldrich (St. Louis, MO, USA), Alfa Aesar (Massachusetts), S.D. Fine Chemicals (India) and Avra chemicals (India). All reactions were performed under inert atmosphere (N_2) unless otherwise noted. The reactions were monitored by thin-layer chromatography (TLC) on precoated silica gel 60 F254 (MerckKGaA) and were visualized under UV light, iodine vapors or by treatment with ninhydrin and bromocresol green reagents. Column chromatographic purifications were performed using silica gel 60–120 mesh size (CDH Laboratory Reagents, India). Proton nuclear magnetic resonance (^{1}H NMR) and ^{13}C NMR spectra were measured on Bruker Advance, 500 MHz spectrometers with tetramethylsilane (TMS) as the internal standard. The NMR solvents used were $CDCl_3$ or DMSO–d_6 as indicated. Chemical shifts were measured in ppm and coupling constants (*J*) were measured in Hz. The following abbreviations are used to describe peak splitting patterns when appropriate: d = doublet, t = triplet, q = quartet, m = multiplet, dd = doublet of doublet, br = broad. Coupling constants J are reported in Hertz (Hz). High resolution mass spectra (HRMS) were recorded at Indian Institute of Technology, Ropar, India, CSIR- Indian

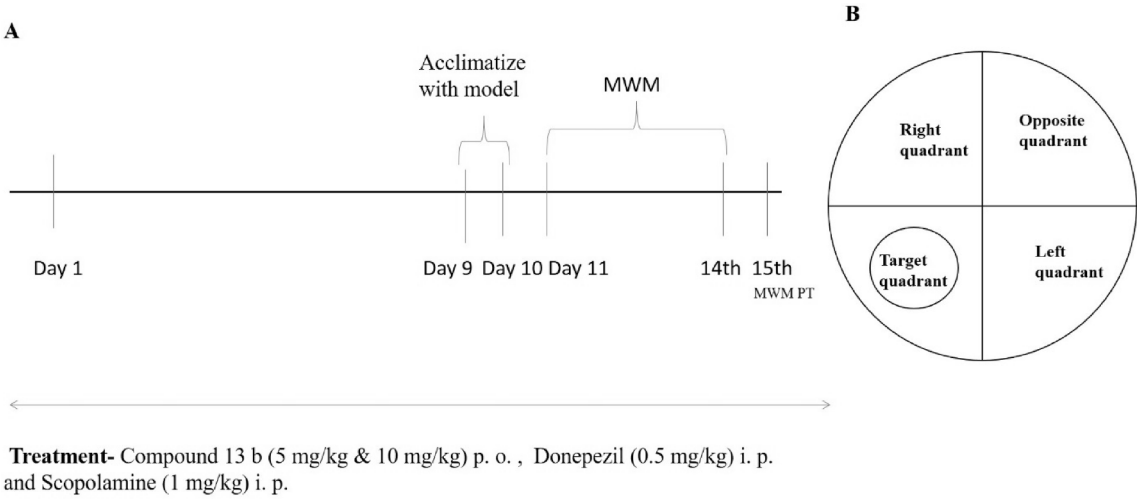

Fig. 11. (**A**) Schematic schedule of experimental design to study the anti-amnestic effect of compound **13b**. (**B**) Outline of the Morris water maze model experiment. I.P.; intraperitoneal, P.O; per os (orally), MWM PT-probe trial of Morris water maze test; MWM- Morris water maze.

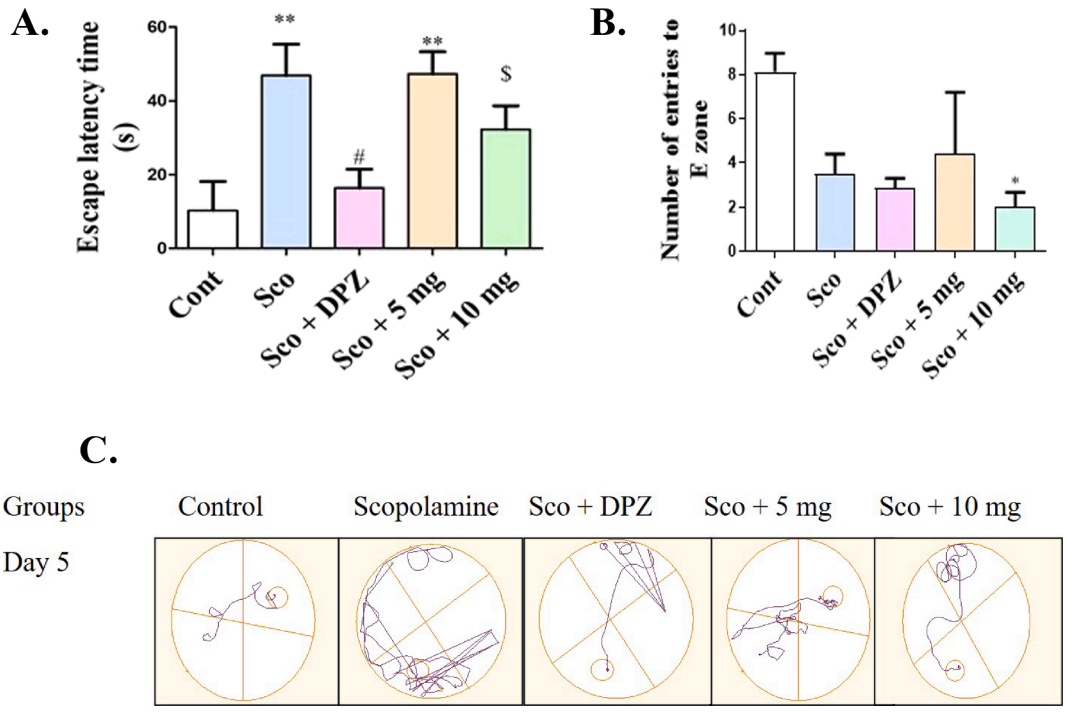

Fig. 12. Scopolamine-induced memory deficit mice model study. (**A**) Escape latency time on Day 5 (**B**) No. of entries in E zone. (**C**) Track diagram on Day 5. Data are expressed as mean ± SEM (n = 7). ** $p < 0.01$, * $p < 0.05$ versus corresponding value in the control in Fig A and vs scopolamine in Fig. B, #$p < 0.01$ vs. scopolamine (Sco) group , \$$p < 0.05$ vs Sco group. (Data recorded through Any Maze software). (Data recorded through Any Maze software).

Institute of Chemical Technology, Hyderabad and North East Institute of Science & Technology (CSIR–NEIST), Jorhat. The HRMS of the halogenated compounds was measured with reference to major isotope *i.e.* ^{35}Cl, has been carried out and reported.

4.1.1. *General procedure for the synthesis of intermediates* ***2e-2g, 2i, 2m-2o***

To a stirring solution of substituted benzyl halide (1.0 equiv, 1 mmol) in ethanol (30 mL), K_2CO_3 (3.0 equiv, 3.0 mmol), the appropriate anhydrous piperazine (4.0 equiv) were added followed by the general procedure in the literature.[40,41] After being refluxed for 4–6 h, the ethanol was evaporated under reduced pressure, and subjected residue was diluted with EtOAc (20 mL) and washed with ice cold water. The aqueous layer was extracted with EtOAc (3 × 20 mL). The combined organic layer was washed with brine, dried over Na_2SO_4, and concentrated to yield the aforementioned compounds **2e-2g, 2i, 2m-2o**, which were used without purification in the next step. The intermediates were characterized with help of ^1H NMR. The NMR spectra's of the synthesized intermediates are matching with the reported values.

4.1.2. *General procedure for the synthesis of target compounds* ***3a-3p***

Into a stirring solution of **FA** (0.2 g, 1.0 equiv.), EDCI. HCl, 0.29 g, 1.5 equiv.), HOBt (0.37 g, 2.5 equiv.), and DIPEA (0.33 g, 2.5 equiv.) were dissolved in dry THF (20 mL). The desired amount of the substituted benzyl piperazine either commercially or synthesized derivative **2a-2p** (0.8 equiv.) was added to the reaction flask and the reaction mixture was stirred under nitrogen atmosphere at rt for 12 h. The progress of chemical reaction was monitored using Hexane/EtOAc as mobile phase. Upon completion of the reaction, THF was removed under reduced pressure, and saturated $NaHCO_3$ solution was slowly added into it. The reaction mixture was extracted with EtOAc (3 × 30 mL), and the combined organic layer was dried over Na_2SO_4, and evaporated under reduced pressure to obtain the crude product. Further purification was carried by column chromatography with the help of hexane/EtOAc.

4.1.2.1. *(E)-1-(4-benzylpiperazin-1-yl)-3-(4-hydroxy-3-methoxyphenyl) prop-2-en-1-one (3a).*

Into a stirring solution of compound **FA** (0.194 g, 1 equiv.) in THF (20 mL), EDCI.HCl (1.5 equiv., 0.29 g), HOBt (2.5 equiv., 0.37 g), **2a** (0.8 equiv. 0.16 g), and DIPEA (2.5 equiv., 0.33 g) were added at room temperature followed by the general procedure as described above. The crude material was purified through column chromatography using silica gel (100–200 mesh size) as a stationary phase and EtOAc:hexane (9:1) as a mobile phase.

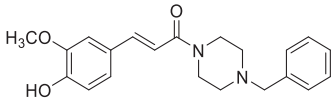

White solid powder, (0.145 g, 75% yield). ^1H NMR (DMSO-d_6, 500 MHz): δ 9.44 (s, 1H, —OH), 7.40 (d, J = 15.2 Hz, 1H, —CH═CH—), 7.34–7.25 (m, 6H), 7.08–7.02 (m, 2H, Ar-H), 6.76 (d, J = 8.0 Hz, 1H, Ar-H), 3.81 (bs, 3H, —OCH_3 of FA), 3.69 (bs, 2H, —CH_2), 3.54–3.50 (m, 4H, pip-H), 2.39–2.34 (m, 4H, pip-H). ^{13}C NMR (DMSO-d_6, 126 MHz): δ 165.2, 148.9, 148.3, 142.7, 138.2, 129.4, 128.6, 127.4, 127.1, 122.9, 115.8, 114.9, 111.6, 62.3, 56.2, 53.7, 52.8, 45.4, 42.1. ESI-HRMS for $C_{21}H_{24}N_2O_3$. $(M+H)^+$ calcd. 353.1865, found 353.1864.

4.1.2.2. *(E)-3-(4-hydroxy-3-methoxyphenyl)-1-(4-(2-methylbenzyl)piperazin-1-yl)prop-2-en-1-one (**3b.HCl**).*

Into a stirring solution of compound **FA** (0.194 g, 1 equiv.) in THF (20 mL), EDCI.HCl (1.5 equiv., 0.29 g), HOBt (2.5 equiv., 0.37 g), **2b** (0.8 equiv. 0.15 g), and DIPEA (2.5 equiv., 0.33 g) were added at room temperature followed by the general procedure as described above. Thus, obtained compound was treated with etherial HCl (2 M in diethyl ether, Sigma Aldrich) to convert into corresponding hydrochloride salt.

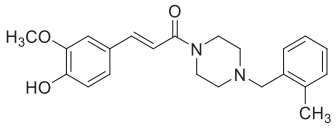

White solid powder, (0.200 g, 69% yield). ^{1}H NMR ($CDCl_3$, 500 MHz): δ 7.60 (d, J = 15.5 Hz, 1H, —CH═CH—), 7.24 (d, J = 7.5 Hz, 1H, Ar-H), 7.19–7.14 (m, 3H, Ar-H), 7.08 (dd, J_1 = 8.5 Hz, J_2 = 2.0 Hz, 1H, Ar-H), 6.98 (d, J = 2.0 Hz, 1H, Ar-H), 6.90 (d, J = 8.5 Hz, 1H, Ar-H), 6.70 (d, J = 15.5 Hz, 1H, —CH═CH—), 3.91 (s, 3H, OCH_3 of FA), 3.72–3.62 (m, 4H, pip-H), 3.48 (s, 2H, CH_2), 2.48 (t, J = 5.0 Hz, 4H, pip-H), 2.37 (s, 3H, CH_3). ^{13}C NMR ($CDCl_3$, 126 MHz): δ 171.1, 165.6, 147.3, 146.7, 142.8, 137.5, 135.8, 130.3, 129.9, 127.8, 127.3, 125.5, 121.8, 114.7, 114.5, 109.9, 60.7, 60.4, 55.9, 21.0, 19.2. ESI-HRMS for $C_{22}H_{26}N_2O_3$. $(M+H)^+$ calcd. 367.2022, found 367.2031.

*4.1.2.3. (E)-3-(4-hydroxy-3-methoxyphenyl)-1-(4-(3-methylbenzyl)piperazin-1-yl)prop-2-en-1-one (**3c.HCl**).* Into a stirring solution of compound **FA** (0.194 g, 1 equiv.) in THF (20 mL), EDCI.HCl (1.5 equiv., 0.29 g), HOBt (2.5 equiv., 0.37 g),**2c** (0.8 equiv. 0.15 g), and DIPEA (2.5 equiv., 0.33 g) were added at room temperature followed by the general procedure as described above. Thus, obtained compound was treated with etherial HCl (2 M in diethyl ether, Sigma Aldrich) to convert into corresponding hydrochloride salt.

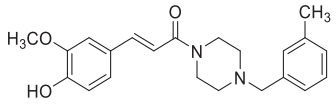

White solid powder, (0.200 g, 69% yield). ^{1}H NMR ($CDCl_3$, 500 MHz): δ 7.62 (d, J = 15.5 Hz, 1H, —CH═CH—), 7.24 (t, J = 6.0 Hz, 1H, Ar-H), 7.16–7.10 (m, 4H, Ar-H), 7.00 (d, J = 5.0 Hz, 1H, Ar-H), 6.93 (d, J = 7.5 Hz, 1H, Ar-H), 6.73 (d, J = 15.5 Hz, 1H, —CH═CH—), 3.94 (s, 3H, OCH_3 of FA), 3.76–3.67 (m, 4H, pip-H), 3.52 (s, 2H, CH_2), 2.50 (d, J = 6.0 Hz, 4H, pip-H), 2.37 (s, 3H, CH_3). ^{13}C NMR (DMSO-d_6, 126 MHz): δ 165.5, 149.2, 148.2, 143.7, 138.5, 132.4, 130.6, 129.8, 129.1, 128.9, 126.8, 123.1, 115.9, 114.0, 111.8, 59.5, 56.2, 21.4. ESI-HRMS for $C_{22}H_{26}N_2O_3$. $(M+H)^+$ calcd. 367.2022, found 367.2013.

*4.1.2.4. (E)-3-(4-hydroxy-3-methoxyphenyl)-1-(4-(4-methylbenzyl)piperazin-1-yl)prop-2-en-1-one (**3d**).* Into a stirring solution of compound **FA** (0.194 g, 1 equiv.) in THF (20 mL), EDCI.HCl (1.5 equiv., 0.29 g), HOBt (2.5 equiv., 0.37 g), **2d** (0.8 equiv. 0.15 g), and DIPEA (2.5 equiv., 0.33 g) were added at room temperature followed by the general procedure as described above.

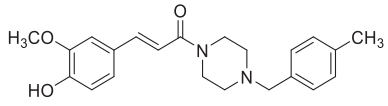

White solid powder, (0.200 g, 68% yield). ^{1}H NMR ($CDCl_3$, 500 MHz): δ 7.62 (d, J = 15.5 Hz, 1H, —CH═CH—), 7.22 (d, J = 8.0 Hz, 2H, Ar-H), 7.16 (d, J = 8.00 Hz, 2H, Ar-H), 7.10 (dd, J_1 = 8.5 Hz, J_2 = 2.0 Hz, 1H Ar-H), 7.00 (d, J = 6.0 Hz, 1H, Ar-H), 6.92 (d, J = 8.0 Hz, 1H, Ar-H), 6.72 (d, J = 15.5 Hz, 1H, —CH═CH—), 3.94 (s, 3H, —OCH_3 of FA), 3.76–3.67 (m, 4H, pip-H), 3.53 (s, 2H, —CH_2-), 2.50 (t, J = 5.0 Hz, 4H, pip-H), 2.36 (s,3H, CH_3). ^{13}C NMR ($CDCl_3$, 126 MHz): δ 165.6, 147.3, 146.6, 142.8, 137.0, 129.1, 129.0, 127.8, 121.8, 114.7, 114.5, 109.8, 62.6, 55.9, 31.9, 29.7, 22.6, 21.1, 14.1. ESI-HRMS for $C_{22}H_{26}N_2O_3$. $(M+H)^+$ calcd. 367.2022, found 367.2018.

*4.1.2.5. (E)-3-(4-hydroxy-3-methoxyphenyl)-1-(4-(3-methoxybenzyl) piperazin-1-yl)prop-2-en-1-one (**3e**).* Into a stirring solution of compound **FA** (0.194 g, 1 equiv.) in THF (20 mL), EDCI.HCl (1.5 equiv., 0.29 g), HOBt (2.5 equiv., 0.37 g) **2e** (0.8 equiv. 0.16 g), and DIPEA (2.5 equiv., 0.33 g) were added at room temperature followed by the general procedure as described above.

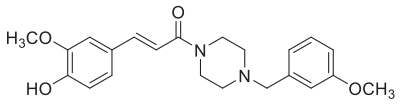

White solid powder, (0.210 g, 69% yield). ^{1}H NMR (DMSO-d_6, 500 MHz): δ 7.55–7.42 (m, 1H, Ar-H), 7.20–7.17 (m, 2H, Ar-H), 7.03–7.01 (m, 1H, Ar-H), 6.92–6.85 (m, 3H, Ar-H), 6.79–6.76 (m, 2H), 3.83 (s, 3H, —OCH_3), 3.73 (s, 3H, —OCH_3), 3.67 (s, 4H, pip-H), 3.44 (s, 2H, CH_2), 2.41 (s, 4H, pip-H). ^{13}C NMR (DMSO-d_6, 126 MHz): δ 166.7, 159.9, 148.7, 147.9, 143.6, 138.7, 129, 127.2, 122.4, 121.4, 115.1, 114.6, 113.4, 112.5, 110.4, 62.3, 55.1, 54.3, 53, 52.5, 47.2, 45.3. ESI-HRMS for $C_{22}H_{26}N_2O_4$. $(M+H)^+$ calcd. 383.1971, found 383.1968.

*4.1.2.6. (E)-3-(4-hydroxy-3-methoxyphenyl)-1-(4-(4-methoxybenzyl) piperazin-1-yl)prop-2-en-1-one (**3f**).* Into a stirring solution of compound **FA** (0.194 g, 1 equiv.) in THF (20 mL), EDCI.HCl (1.5 equiv., 0.29 g), HOBt (2.5 equiv., 0.37 g), **2f** (0.8 equiv. 0.16 g), and DIPEA (2.5 equiv., 0.33 g) were added at room temperature followed by the general procedure as described above.

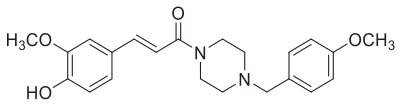

White solid powder, (0.210 g, 69% yield). ^{1}H NMR ($CDCl_3$, 500 MHz): δ 7.61 (d, J = 15.3 Hz, 1H, —CH═CH—), 7.25 (d, J = 8.3 Hz, 2H, Ar-H), 7.09 (d, J = 8.2 Hz, 1H, Ar-H), 6.99 (s, 1H, Ar-H), 6.92–6.87 (m, 3H, Ar-H), 6.71 (d, J = 15.3 Hz, 1H, —CH═CH—), 3.93 (s, 3H, OCH_3 of FA), 3.82–3.69 (m, 7H, —OCH_3 and 4 pip-H merged), 3.53 (s, 2H, CH_2), 2.51 (s, 4H, pip-H). ^{13}C NMR ($CDCl_3$, 126 MHz): δ 165.6, 159.0, 147.4, 146.7, 142.9, 130.5, 127.8, 121.9, 114.8, 114.4, 113.7, 109.9, 62.1, 55.9, 55.2, 53.1, 52.5, 45.6, 42.0, 29.6. ESI-HRMS for $C_{22}H_{26}N_2O_4$. $(M+H)^+$ calcd. 383.1971, found 383.1970.

*4.1.2.7. (E)-1-(4-(2-chlorobenzyl)piperazin-1-yl)-3-(4-hydroxy-3-methoxyphenyl)prop-2-en-1-one (**3g.HCl**).* Into a stirring solution of compound **FA** (0.194 g, 1 equiv.) in THF (20 mL), EDCI.HCl (1.5 equiv., 0.29 g), HOBt (2.5 equiv., 0.37 g), **2g** (0.8 equiv. 0.17 g), and DIPEA (2.5 equiv., 0.33 g) were added at room temperature followed by the general procedure as described above. Thus, obtained compound was treated with etherial HCl (2 M in diethyl ether, Sigma Aldrich) to convert into corresponding hydrochloride salt.

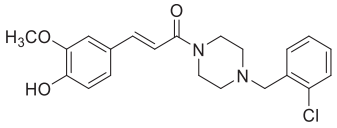

White solid powder, (0.214 g, 69% yield). ^{1}H NMR ($CDCl_3$, 500 MHz): δ 7.62 (d, J = 15.3 Hz, 1H, —CH═CH—), 7.49 (d, J = 7.5 Hz, 1H, Ar-H), 7.39 (dd, J_1 = 7.8 Hz, J_2 = 1.3 Hz, 1H, Ar-H), 7.26–7.21 (m, 2H, merged with $CDCl_3$, Ar-H), 7.12–7.10 (m, 1H, Ar-H), 7.01–7.12 (m, 1H, Ar-H), 6.92 (d, J = 8.2 Hz, 1H, Ar-H), 6.73 (d, J = 15.3 Hz, 1H, —CH═CH—), 3.94 (s, 3H, OCH_3 of FA), 3.77 (s, 4H, pip-H), 3.68 (s, 2H, CH_2), 2.58 (t, J = 5.0 Hz, 4H, pip-H). ^{13}C NMR ($CDCl_3$, 126 MHz): δ 165.6, 147.3, 146.7, 142.9, 135.3, 134.4, 130.8, 129.5, 128.4, 127.8, 126.6, 121.8, 114.7, 114.5, 109.8, 59.1, 56.0, 29.7. ESI-HRMS for $C_{21}H_{23}ClN_2O_3$. $(M+H)^+$ calcd. 387.1475, found 387.1471.

*4.1.2.8. (E)-1-(4-(3-chlorobenzyl)piperazin-1-yl)-3-(4-hydroxy-3-methoxyphenyl)prop-2-en-1-one (**3h**).* Into a stirring solution of compound **FA** (0.194 g, 1 equiv.) in THF (20 mL), EDCI.HCl (1.5 equiv., 0.29 g), HOBt (2.5 equiv., 0.37 g), **2h** (0.8 equiv. 0.17 g), and DIPEA (2.5 equiv., 0.33 g) were added at room temperature followed by the general

procedure as described above.

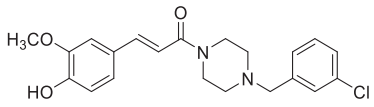

White solid powder, (0.214 g, 71% yield). ^{1}H NMR ($CDCl_3$, 500 MHz): δ 7.61 (d, J = 15.3 Hz, 1H, —CH═CH—), 7.36 (s, 1H, Ar-H), 7.28–7.21 (m, 3H, Ar-H), 7.10 (d, J = 8.0 Hz, 1H, Ar-H), 6.99 (s, 1H, Ar-H), 6.92 (d, J = 8.2 Hz, 1H, Ar-H), 6.70 (d, J = 15.3 Hz, 1H, —CH═CH—), 3.92 (s, 3H, —OCH_3), 3.76–3.68 (m, 4H, pip-H), 3.52 (s, 2H, —CH_2), 2.49 (t, J = 5.5 Hz, 4H, pip-H). ^{13}C NMR ($CDCl_3$, 126 MHz): δ 165.7, 147.4, 146.7, 143.0, 139.8, 134.3, 129.6, 129.0, 127.7, 127.5, 127.1, 121.9, 114.8, 114.3, 109.9, 62.2, 55.9. ESI-HRMS for $C_{21}H_{23}ClN_2O_3$. $(M+H)^+$ calcd. 387.1475, found 387.1470.

*4.1.2.9. (E)-1-(4-(4-chlorobenzyl)piperazin-1-yl)-3-(4-hydroxy-3-methoxyphenyl)prop-2-en-1-one **(3i)***. Into a stirring solution of compound **FA** (0.194 g, 1 equiv.) in THF (20 mL), EDCI.HCl (1.5 equiv., 0.29 g), HOBt (2.5 equiv., 0.37 g), **2i** (0.8 equiv. 0.17 g), and DIPEA (2.5 equiv., 0.33 g) were added at room temperature followed by the general procedure as described above.

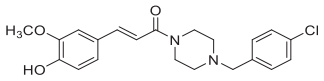

White solid powder, (0.214 g, 70% yield). ^{1}H NMR ($CDCl_3$, 500 MHz): δ 7.62 (d, J = 15.3 Hz, 1H, —CH═CH—), 7.32–7.27 (m, 4H, Ar-H), 7.10 (dd, J_1 = 8.0 Hz, J_2 = 2.0 Hz, 1H, Ar-H), 6.99 (d, J = 2.0 Hz, 1H), 6.62 (d, J = 8.0 Hz, 1H, Ar-H), 6.71 (d, J = 15.3 Hz, 1H, —CH═CH—), 3.92 (s, 3H, OCH_3), 3.75–3.67 (m, 4H, pip-H), 3.51 (s, 2H, —CH_2), 2.48 (t, J = 5.5 Hz, 4H, pip-H). ^{13}C NMR ($CDCl_3$, 126 MHz): δ 165.7, 147.4, 146.7, 143.0, 136.1, 133.0, 130.3, 128.5, 127.7, 121.8, 114.8, 114.3, 109.9, 62.0, 55.9. ESI-HRMS for $C_{21}H_{23}ClN_2O_3$. $(M+H)^+$ calcd. 387.1475, found 387.1477.

*4.1.2.10. (E)-1-(4-(2-fluorobenzyl)piperazin-1-yl)-3-(4-hydroxy-3-methoxyphenyl)prop-2-en-1-one **(3j.HCl)***. Into a stirring solution of compound **FA** (0.194 g, 1 equiv.) in THF (20 mL), EDCI.HCl (1.5 equiv., 0.29 g), HOBt (2.5 equiv., 0.37 g), **2j** (0.8 equiv. 0.16 g), and DIPEA (2.5 equiv., 0.33 g) were added at room temperature followed by the general procedure as described above. Thus, obtained compound was treated with etherial HCl (2 M in diethyl ether, Sigma Aldrich) to convert into corresponding hydrochloride salt.

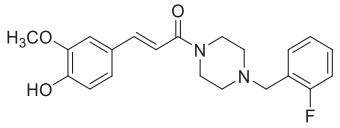

White solid powder, (0.216 g, 71% yield). ^{1}H NMR ($CDCl_3$, 500 MHz): δ 7.58 (d, J = 15.0 Hz, 1H, —CH═CH—), 7.35 (td, J_1 = 7.5 Hz, J_2 = 2.0 Hz, 1H, Ar-H), 7.25–7.22 (m, 1H, Ar-H), 7.10 (td, J_1 = 8.0 Hz, J_2 = 1.0 1H, Ar-H), 7.05–7.00 (m, 2H, Ar-H), 6.96 (d, J = 5.5 Hz, 1H, Ar-H), 6.87 (d, J = 8.0 Hz, 1H, Ar-H), 6.68 (d, J = 15.5 Hz, 1H, —CH═CH—), 3.86 (s, 3H, OCH_3 of FA), 3.75–3.72 (m, 4H, pip-H), 3.62 (bs, 2H, CH_2), 2.52 (t, J = 5.0 Hz, 4H, pip-H). ^{13}C NMR ($CDCl_3$, 126 MHz): δ 165.7, 162.3, 160.4, 147.7, 147.0, 143.1, 131.6, 131.6, 129.1, 129.1, 127.5, 123.9, 123.9, 123.8, 123.7, 121.9, 115.4, 115.2, 115.0, 114.1, 110.0, 67.9, 55.9, 55.0, 55.0, 52.9, 52.4, 25.5. ESI-HRMS for $C_{21}H_{23}FN_2O_3$. $(M+H)^+$ calcd. 371.1771, found 371.1769.

*4.1.2.11. (E)-1-(4-(3-fluorobenzyl)piperazin-1-yl)-3-(4-hydroxy-3-methoxyphenyl)prop-2-en-1-one **(3k.HCl)***. Into a stirring solution of compound **FA** (0.194 g, 1 equiv.) in THF (20 mL), EDCI.HCl (1.5 equiv., 0.29 g), HOBt (2.5 equiv., 0.37 g), **2k** (0.8 equiv. 0.15 g), and DIPEA (2.5 equiv., 0.33 g) were added at room temperature followed by the general procedure as described above. Thus, obtained compound was treated with etherial HCl (2 M in diethyl ether, Sigma Aldrich) to convert into corresponding hydrochloride salt.

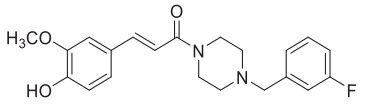

White solid powder, (0.216 g, 73% yield). ^{1}H NMR ($CDCl_3$, 500 MHz): δ 7.62 (d, J = 15.5 Hz, 1H, —CH═CH—), 7.32–7.28 (m, 1H, Ar-H), 7.14–7.09 (m, 3H, Ar-H), 7.01–7.7.00 (m, 2H, Ar-H), 6.92 (d, J = 8.5 Hz, 1H, Ar-H), 6.71 (d, J = 15.5 Hz, 1H, —CH═CH—), 3.94 (s, 3H, —OCH_3 of FA), 3.79–3.71 (m, 4H, pip-H), 3.58 (s, 2H, —CH_2), 2.54 (s, 4H, pip-H). ^{13}C NMR (DMSO-d_6, 126 MHz): δ 168.8, 165.2, 148.9, 148.2, 142.7, 138, 129, 127.4, 127.1, 123, 121.5, 115.8, 114.9, 111.6, 61.8, 56.2, 49.0 ESI-HRMS for $C_{21}H_{23}FN_2O_3$. $(M+H)^+$ calcd. 371.1771, found 371.1776.

*4.1.2.12. (E)-1-(4-(4-fluorobenzyl)piperazin-1-yl)-3-(4-hydroxy-3-methoxyphenyl)prop-2-en-1-one **(3l.HCl)***. Into a stirring solution of compound **FA** (0.194 g, 1 equiv.) in THF (20 mL), EDCI.HCl (1.5 equiv., 0.29 g), HOBt (2.5 equiv., 0.37 g), **2l** (0.8 equiv. 0.167 g), and DIPEA (2.5 equiv., 0.33 g) were added at room temperature followed by the general procedure as described above. Thus, obtained compound was treated with etherial HCl (2 M in diethyl ether, Sigma Aldrich) to convert into corresponding hydrochloride salt.

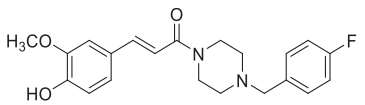

White solid powder, (0.210 g, 69% yield). ^{1}H NMR (DMSO-d_6, 500 MHz): δ 7.59 (d, J = 15.5 Hz, 1H, —CH═CH—), 7.29–7.27 (m, 2H, Ar-H), 7.07 (dd, J_1 = 8.5 Hz, J_2 = 2.0 Hz, 1H, Ar-H), 7.08–6.97 (m, 3H, Ar-H), 6.90 (d, J = 8.0 Hz, 1H, Ar-H), 6.70 (d, J = 15.0 Hz, 1H, —CH═CH—), 3.91 (s, 3H, —OCH_3 of FA), 3.65–3.73 (bs, 4H, pip-H), 3.49 (s, 2H, CH_2), 2.46 (t, J = 5.0 Hz, 4H, pip-H). ^{13}C NMR (DMSO-d_6, 126 MHz): δ 165.7, 163.1, 161.18, 147.4, 146.7, 143, 130.6, 130.6, 127.8, 121.8, 115.2, 115.1, 114.7, 114.3, 109.9, 62, 55.9, 53.1, 52.7, 31.9, 29.7, 27, 19.7, 14.1. ESI-HRMS for $C_{21}H_{23}FN_2O_3$. $(M+H)^+$ calcd. 371.1771, found 371.1775.

*4.1.2.13. 4.1.2.13.(E)-2-((4-(3-(4-hydroxy-3-methoxyphenyl)acryloyl) piperazin-1-yl)methyl) benzonitrile **(3m)***. Into a stirring solution of compound **FA** (0.194 g, 1 equiv.) in THF (20 mL), EDCI.HCl (1.5 equiv., 0.29 g), HOBt (2.5 equiv., 0.37 g), **2m** (0.8 equiv. 0.161 g), and DIPEA (2.5 equiv., 0.33 g) were added at room temperature followed by the general procedure as described above. The crude material was purified by column chromatography using silica gel (100–200 mesh size) as a stationary phase with help of EtOAc:hexane(9:1) as mobile phase.

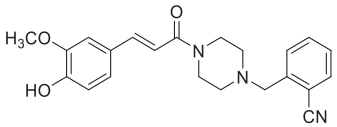

White solid powder, (0.213 g, 71% yield). ^{1}H NMR ($CDCl_3$, 500 MHz): δ 7.69–7.54 (m, 4H, Ar-H), 7.40 (t, J = 8.5 Hz, 1H, Ar-H), 7.11–7.09 (m, 1H, Ar-H), 7.00 (bs, 1H, Ar-H), 6.92 (d, J = 7.75 Hz, 1H, Ar-H), 6.72 (d, J = 15.5 Hz, 1H, —CH═CH—), 3.93 (s, 3H, OCH_3), 3.75–3.69 (m, 6H, pip-H, —CH_2), 2.57 (s, 4H, pip-H). ^{13}C NMR ($CDCl_3$, 126 MHz): δ 165.7, 147.3, 146.7, 143.0, 141.8, 133.1, 132.6, 130.1, 127.8, 127.8, 121.9, 117.7, 114.7, 114.4, 113.1, 109.8, 60.3, 56.0. ESI-

HRMS for $C_{22}H_{23}N_3O_3$. $(M+H)^+$ calcd. 378.1818, found 378.1814.

*4.1.2.14. (E)-3-((4-(3-(4-hydroxy-3-methoxyphenyl)acryloyl)piperazin 1yl)methyl)benzonitrile (**3n**).* Into a stirring solution of compound **FA** (0.194 g, 1 equiv.) in THF (20 mL), EDCI.HCl (1.5 equiv., 0.29 g), HOBt (2.5 equiv., 0.37 g), **2n** (0.8 equiv. 0.161 g), and DIPEA (2.5 equiv., 0.33 g) were added at room temperature followed by the general procedure as described above.

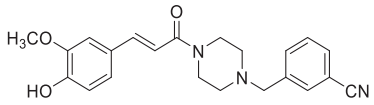

Brown solid powder, (0.213 g, 70% yield). ^{1}H NMR ($CDCl_3$, 500 MHz): δ 7.69–7.58 (m, 4H, Ar-H), 7.45 (t, J = 8.5 Hz, 1H, Ar-H), 7.10 (dd, J_1 = 8.0 Hz, J_2 = 2.0 Hz, 1H, Ar-H), 7.00 (d, J = 2.0 Hz, 1H, Ar-H), 6.92 (d, J = 8.15 Hz, 1H, Ar-H), 6.71 (d, J = 15.5 Hz, 1H, —CH═CH—), 3.94 (s, 3H, OCH_3), 3.76 (s, 4H, pip-H), 3.57 (s, 2H, CH_2), 2.49 (t, J = 5.5 Hz, 4H, pip-H) . ^{13}C NMR ($CDCl_3$, 126 MHz): δ 165.7, 147.4, 146.7, 143.1, 139.5, 133.3, 132.3, 131.0, 129.1, 121.8, 118.8, 114.7, 112.5, 109.9, 61.8, 55.9. ESI-HRMS for $C_{22}H_{23}N_3O_3$. $(M+H)^+$ calcd. 378.1818, found 378.1816.

*4.1.2.15. (E)-4-((4-(3-(4-hydroxy-3-methoxyphenyl)acryloyl)piperazin-1-yl)methyl)benzonitrile (**3o.HCl**).* Into a stirring solution of compound **FA** (0.194 g, 1 equiv.) in THF (20 mL), EDCI.HCl (1.5 equiv., 0.29 g), HOBt (2.5 equiv., 0.37 g) **2o** (0.8 equiv. 0.161 g), and DIPEA (2.5 equiv., 0.33 g) were added at room temperature followed by the general procedure as described above. Thus, obtained compound was treated with etherial HCl (2 M in diethyl ether, Sigma Aldrich) to convert into corresponding hydrochloride salt.

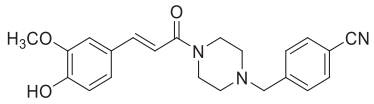

White solid powder, (0.195 g, 65% yield). ^{1}H NMR (DMSO-d_6, 500 MHz): δ 9.52 (s, 1H, OH), 8.14 (s, 1H, Ar-H), 7.84 (d, J = 8.0 Hz, 1H, Ar-H), 7.62 (d, J = 8.0 Hz, 1H, Ar-H), 7.50–7.46 (m, 2H), 7.33 (bs, 1H), 7.14–7.06 (m, 2H), 6.80 (d, J = 8.0 Hz, 1H, Ar-H), 4.51–4.25 (m, 4H, pip-H), 3.83 (m, 3H, OCH_3 of FA), 3.61–3.56 (m, 4H, pip-H), 3.17 (s, 2H, CH_2). ^{13}C NMR (DMSO-d_6, 126 MHz): δ 168.4, 166.1, 149.8, 149.5, 140.1, 139.6, 138.3, 129.1, 129, 128.5, 128.1, 127.2, 127.1, 113.2, 110.8, 67.2, 58.2, 55.9, 51.6, 47.8, 43.3. ESI-HRMS for $C_{22}H_{23}N_3O_3$. $(M+H)^+$ calcd. 378.1818, found 378.1826.

*4.1.2.16. (E)-3-(4-hydroxy-3-methoxyphenyl)-1-(4-(3-nitrobenzyl)piperazin-1-yl)prop-2-en-1-one (**3p.HCl**).* Into a stirring solution of compound **FA** (0.194 g, 1 equiv.) in THF (20 mL), EDCI.HCl (1.5 equiv., 0.29 g), HOBt (2.5 equiv., 0.37 g), **2p** (0.8 equiv. 0.201 g), and DIPEA (2.5 equiv., 0.33 g) were added at room temperature followed by the general procedure as described above. Thus, obtained compound was treated with etherial HCl (2 M in diethyl ether, Sigma Aldrich) to convert into corresponding hydrochloride salt.

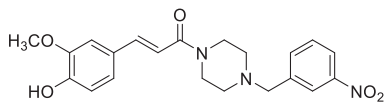

Yellow solid powder, (0.251 g, 70% yield). ^{1}H NMR (DMSO-d_6, 500 MHz): δ 9.90 (bs, 1H), 9.43 (bs, 1H, —OH), 7.67 (d, J = 8.5 Hz, 2H, Ar-H), 7.42–7.30 (m, 4H, Ar-H), 7.08–7.02 (m, 2H), 6.77 (d, J = 8.5 Hz, 1H, Ar-H), 3.82 (s, 3H, —OCH_3 of FA), 3.76–3.63 (m, 4H, pip-H), 3.19 (bs, 2H), 2.53 (bs, 4H, pip-H, merged with DMSO-d_6). ^{13}C NMR (DMSO-d_6, 126 MHz): δ 168.8, 165.3, 148.9, 148.2, 142.7, 137.9, 128.9, 127.5, 127.1, 122.9, 121.6, 115.8, 114.8, 111.6, 61.8, 56.5, 56.2, 55.2, 53.6, 52.9, 18.9. ESI-HRMS for $C_{21}H_{23}ClN_2O_3$. $(M+H)^+$ calcd. 398.1716, found 398.1719.

*4.1.3. General procedure for the synthesis of 3-((tert-butoxycarbonyl) amino)propanoic acid (**5**)*

Into a stirring solution alanine (0.8 g, 9.09 mmol) in DCM (30 mL), $(Boc)_2O$ (2.37 g, 10.90 mmol) and NaOH (0.29 g, 7.27 mmol) were added at 0 °C. The reaction mixture was stirred at room temperature for 12 h and was extracted with DCM (3 × 30 mL), washed with water, dried over Na_2SO_4, filtered, and concentrated in vacuo. The crude material was purified by column chromatography over silica gel (hexane/EtOAc, 9.0:1.0) to give compound **5.** White solid powder, yield 80%. ^{1}H NMR ($CDCl_3$, 500 MHz): δ 6.26 (s, 1H), 5.12 (s, 1H), 3.41 (d, J = 5.5 Hz, 2H), 2.59–2.54 (m, 2H), 1.47 (s, 9H).

*4.1.4. General procedure for the synthesis of intermediates **6a-6c***

Into a stirring solution of compound **5** (0.20 g, 1 mmol) in DCM (20 mL), substituted amine (0.19 g, 0.8 mmol), HOBt, (0.37 g, 2.5 mmol), 1-Ethyl-3-EDCI.HCl (0.29 g, 1.5 mmol) and DIPEA (0.33 g, 2.5 mmol) were added at room temperature. After the reaction mixture was stirred for 8–10 h, a saturated brine solution was added into the reaction mixture, and it was extracted with DCM (3 × 30 mL). The combined organic layer was dried in vacuum, and finally purified by silica gel column chromatography to yield compound (**6a-6c**).

*4.1.4.1. tert-butyl (3-oxo-3-(phenylamino)propyl)carbamate (**6a**).* Into a stirring solution of compound **5** (1 equiv. 0.189 g) in THF (20 mL), EDCI. HCl (1.5 equiv., 0.29 g), HOBt (2.5 equiv., 0.37 g), aniline (0.8 equiv., 0.074 g) and DIPEA (2.5 equiv., 0.33 g) were added at room temperature followed by the general procedure as described above.

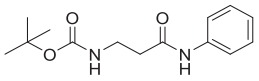

White solid powder, yield (0.225 g, 85%). ^{1}H NMR (DMSO-d_6, 500 MHz): δ 10.02 (bs, 1H –NH), 09.97 (s, 1H –NH). 7.88 (d, J = 8.5 Hz, 2H, Ar-H), 7.56 (d, J = 8.0 Hz, 2H, Ar-H), 7.33 (t, J = 6.5 Hz, 1H, Ar-H), 3.66 (t, J = 6.5 Hz, 2H, methylene protons), 3.19 (t, J = 7.0 Hz, 2H, methylene protons), 1.51 (s, 9H, Boc protons).

*4.1.4.2. tert-butyl (3-((3-methoxyphenyl)amino)-3-oxopropyl)carbamate (**6b**).* Into a stirring solution of compound **5** (1 equiv. 0.189 g) in THF (20 mL), EDCI.HCl (1.5 equiv., 0.29 g), HOBt (2.5 equiv., 0.37 g), m-anisidine (0.8 equiv. 0.098 g), and DIPEA (2.5 equiv., 0.33 g) were added at room temperature followed by the general procedure as described above.

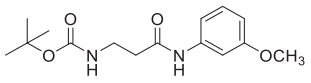

White solid powder, yield (0.242 g, 82%). ^{1}H NMR ($CDCl_3$ 500 MHz): δ 7.81 (q, J_1 = 9.5 Hz, J_2 = 7.0 Hz, 1H), 7.48–7.45 (m, 1H, Ar-H), 7.30 (bs, 1H Ar-H), 7.22 (t, J = 8.0 Hz, 2H Ar-H), 7.03 (d, J = 7.5 Hz 1H, Ar-H), 6.68 (dd, J_1 = 6.5 Hz, J_2 = 1.5 Hz, 1H Ar-H), 3.81 (s, 3H, —OCH_3), 3.49 (q, J_1 = 12.0 Hz, J_2 = 6.0 Hz, 2H, methylene protons), 2.62 (t, J = 6.5 Hz, 2H, methylene protons), 1.44 (s, 9H, boc protons).

*4.1.4.3. tert-butyl (3-((4-chlorophenyl)amino)-3-oxopropyl)carbamate (**6c**).* Into a stirring solution of compound **5** (1.0 equiv. 0.180 g) in THF (20 mL), EDCI.HCl (1.5 equiv., 0.29 g), HOBt (2.5 equiv., 0.37 g), p-chloroaniline (0.8 equiv. 0.10 g), and DIPEA (2.5 equiv., 0.33 g) were added at room temperature followed by the general procedure as described above.

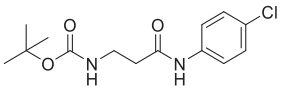

Brown solid powder, yield (0.230 g, 81%). ^{1}H NMR (DMSO-d_6, 500 MHz): δ 7.98 (d, J = 8.5 Hz, 1H, Ar-H), 7.72 (d, J = 8.5 Hz, 1H, Ar-H), 7.62 (d, J = 9.0 Hz, 1H, Ar-H), 7.54 (t, J = 7.0 Hz, 1H, Ar-H), 7.41 (t, J = 6.5 Hz, 1H, Ar-H), 7.33 (d, J = 8.5 Hz, 1H, Ar-H), 3.20 (t, J = 6.5 Hz, 2H, methylene protons), 3.20 (t, J = 6.0 Hz, 2H, methylene protons), 1.37 (s, 9H, boc protons).

*4.1.5. General procedure for the synthesis of intermediates **7a-7c***

Into a stirring solution of compound **6a-6c** (0.2 g, 1 mmol) in DCM (30 mL), TFA (15 mL) was added slowly at room temperature, and the reaction mixture was stirred for 6 h. The unreacted TFA and solvent DCM were removed in vacuo, and thus formed salt was washed with diethyl ether. To the resultant mixture saturated solution of sodium bicarbonate was added, and it was extracted with dichloromethane (50 × 3 mL). The combined organic layer was dried over Na_2SO_4, filtered, and evaporated in vacuo to provide the compound **7a-7c**, which were subjected to next reaction without further purification.

*4.1.6. General procedure for synthesis of target compounds **8a-8c** and **13a-13c***

Into a stirring solution of **FA** (0.3 g, 1.54 mmol) in dry THF (10 mL), HOBt (0.52 g, 3.86 mmol), EDCI.HCl (0.35 g, 2.31 mmol) and DIPEA (0.49 g, 3.86 mmol) were added. The reaction was stirred at room temperature for 15 min. Finally, substituted amine (1.0 equiv.) was added, and the reaction mixture was allowed to stir overnight at room temperature. The progress of the reaction was monitored by TLC. After completion of the reaction, the saturated $NaHCO_3$ solution was added slowly into it. The mixture was extracted with ethyl acetate (3 × 50 mL), and the combined organic layer was washed with brine, dried over Na_2SO_4 and concentrated under vacuum. The residue was subjected to silica gel chromatography or crystallization to afford the aforementioned target compounds.

*4.1.6.1. (E)-3-(4-hydroxy-3-methoxyphenyl)-N-(3-oxo-3-(phenylamino) propyl) acrylamide (**8a**).* Into a stirring solution of compound **FA** (0.3 g, 1.54 equiv.) in THF (20 mL), EDCI.HCl (2.31 equiv., 0.35 g), HOBt (3.86 equiv., 0.52 g), **7a** (0.8 equiv. 0.131 g), and DIPEA (2.5 equiv., 0.33 g) were added at room temperature followed by the general procedure as described above.

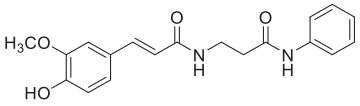

White solid powder, yield (0.128 g, 76%). ^{1}H NMR (DMSO-d_6, 500 MHz): δ 10.10 (s, 1H, —OH), 9.43 (s, 1H, –NH), 8.06 (t, J = 11.5 Hz, 1H, –NH), 7.64 (d, J = 9.0 Hz, 2H, Ar-H), 7.36–7.30 (m, 3H, Ar-H), 7.11 (d, J = 2.0 Hz, 1H, Ar-H), 6.97 (dd, J_1 = 8.0 Hz, J_2 = 1.5 Hz, 1H, Ar-H), 6.78 (d, J = 8.5 Hz, 1H), 6.48 (d, J = 15.5 Hz, 1H, —CH═CH—), 3.79 (s, 3H, —OCH_3), 3.45 (q, J_1 = 12.5 Hz, J_2 = 6.5 Hz, 2H, methylene protons), 2.55 (t, J = 6.5 Hz, 2H, methylene protons). ^{13}C NMR (DMSO-d_6, 126 MHz): δ 166.4, 149.4, 148.8, 148.2, 140.0, 137.2, 135.9, 129.9, 128.7, 126.7, 123.7, 122.2, 122.1, 118.9, 116.1, 115.4, 111.3, 56.0, 43.5. ESI-HRMS for $C_{21}H_{23}ClN_2O_3$. $(M+H)^+$ calcd. 341.1501, found 341.1497.

*4.1.6.2. (E)-3-(4-hydroxy-3-methoxyphenyl)-N-(3-((3-methoxyphenyl) amino)-3-oxopropyl)acrylamide (**8b**).* Into a stirring solution of compound **FA** (0.3 g, 1.54 equiv.) in THF (20 mL), EDCI.HCl (2.31 equiv., 0.35 g), HOBt (3.86 equiv., 0.52 g), **7b** (0.8 equiv. 0.155 g), and DIPEA (2.5 equiv., 0.33 g) were added at room temperature followed by the general procedure as described above.

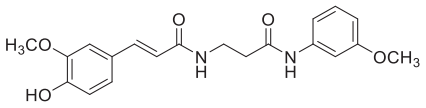

White solid powder, (0.154 g, 71% yield). ^{1}H NMR (DMSO-d_6, 500 MHz): δ 9.44 (bs, 1H, –NH), 8.08 (s, 1H, –NH), 7.34–7.30 (m, 2H, Ar-H), 7.20–7.11 (m, 4H, Ar-H), 6.98 (dd, J_1 = 8.0 Hz, J_2 = 2.5 Hz, 1H, Ar-H), 6.78 (d, J = 8.0 Hz, 1H, Ar-H), 6.61 (dd, J_1 = 8.0 Hz, J_2 = 3.0 Hz, 1H, Ar-H), 6.47 (d, J = 15.5 Hz, 1H, —CH═CH—), 3.83–3.79 (m, 3H, —OCH_3), 3.71 (s, 3H, —OCH_3), 3.45 (q, J_1 = 12.5 Hz, J_2 = 6.5 Hz, 2H, methylene protons), 2.54 (t, J = 6.5 Hz, 2H, methylene protons). ^{13}C NMR (DMSO-d_6, 126 MHz): δ 169.2, 166.1, 148.7, 148.2, 139.8, 136.6, 127.6, 126.8, 123.0, 122.0, 121.3, 119.2, 118.6, 116.1, 112.1, 111.8, 111.3, 56.0, 42.7, 25.6. ESI-HRMS for $C_{20}H_{22}N_2O_5$. $(M+H)^+$ calcd. 371.1607, found 371.1605.

*4.1.6.3. 4.1.6.3. (E)-N-(3-((4-chlorophenyl)amino)-3-oxopropyl)-3-(4-hydroxy-3-methoxyphenyl) acrylamide (**8c**).* Into a stirring solution of compound **FA** (0.3 g, 1.54 equiv.) in THF (20 mL), EDCI.HCl (2.31 equiv., 0.35 g), HOBt (3.86 equiv., 0.52 g), **7c** (0.8 equiv. 0.158 g), and DIPEA (2.5 equiv., 0.33 g) were added at room temperature followed by the general procedure as described above.

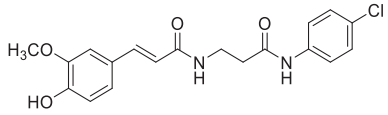

White solid powder, (0.167 g, 74% yield). ^{1}H NMR (DMSO-d_6, 500 MHz): δ 9.97 (bs, 1H —OH), 9.43 (s, 1H, –NH proton), 8.08 (t, J = 5.5 Hz, 1H, –NH proton), 7.60 (d, J = 8.0 Hz, 2H, Ar-H), 7.33–7.27 (m, 3H, Ar-H), 7.11–6.97 (m, 3H, Ar-H), 6.77 (d, J = 8.0 Hz, 1H Ar-H), 6.47 (d, J = 15.5 Hz, 1H, —CH═CH—), 3.79 (s, 3H, —OCH_3), 3.45 (q, J_1 = 8.0 Hz, J_2 = 2.5 Hz, 2H, methylene protons), 2.55 (t, J = 6.5 Hz, 2H, methylene protons). ^{13}C NMR (DMSO-d_6, 126 MHz): δ 169.9, 166.0, 148.7, 148.2, 139.6, 139.4, 129.1, 126.8, 123.5, 122.0, 119.5, 119.3, 116.0, 111.1, 55.9, 36.8, 35.6. ESI-HRMS for $C_{19}H_{19}ClN_2O_4$. $(M+H)^+$ calcd. 375.1112, found 375.1115.

*4.1.7. General procedure for synthesis of intermediate **11a-11c***

Into a stirring solution of Boc-glycine (0.3 g, 2.55 mmol) in THF (20 mL), substituted tryptamine (0.4 g, 2.55 mmol), EDCI.HCl, 0.97 g, 4.59 mmol), HOBt, 0.512 g, 3.82 mmol), and N,*N*-Diisopropylethylamine (DIPEA, 0.15 g, 2.55 mmol) were added at room temperature. After the reaction was stirred for 12 h, a diluted solution of HCl was added into the reaction mixture, and it was extracted with EtOAc (3 × 50 mL). The combined organic layer was washed with brine and finally purified by silica gel column chromatography (EtOAc/Hexane, 1:1) to get aforementioned product.

*4.1.7.1. tert-butyl (2-((2-(1H-indol-3-yl)ethyl)amino)-2-oxoethyl)carbamate (**11a**).* Into a stirring solution of compound *tert*-butoxycarbonyl) glycine (1 equiv. 0.175 g) in THF (20 mL), EDCI.HCl (1.5 equiv., 0.29 g), HOBt (2.5 equiv., 0.37 g), Tryptamine (0.8 equiv. 0.128 g), and DIPEA (2.5 equiv., 0.33 g) were added at room temperature followed by the general procedure as described above.

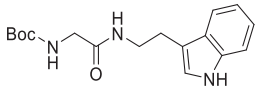

Brown solid powder, yield (0.190 g, 75%). ^{1}H NMR (DMSO-d_6, 500 MHz): δ 10.80 (bs, 1H –NH), 7.85 (t, J = 5.5 Hz, 1H, –NH), 7.52 (d, J = 8.0 Hz, 1H, –NH), 7.32 (d, J = 8.5 Hz, 1H, Ar-H), 7.13 (bs, 1H Ar-H), 7.06 (t, J = 8.0 Hz, 1H, Ar-H), 6.97 (t, J = 7.5 Hz, 1H, Ar-H), 6.91 (t,

$J = 6.0$ Hz, 1H, Ar-H), 3.50 (d, $J = 8.5$ Hz, 2H, methylene protons), 3.34 (q, $J_1 = 7.0$ Hz, $J_2 = 6.5$, 2H, methylene protons), 2.80 (t, $J = 6.5$ Hz, 2H, methylene protons), 1.38 (s, 9H, boc protons).

4.1.7.2. tert-butyl(2-((2-(5-methoxy-1H-indol-3-yl)ethyl)amino)-2-oxoethyl)carbamate (11b). Into a stirring solution of compound *tert*-butoxycarbonyl)glycine (1 equiv. 0.175 g) in THF (20 mL), EDCI.HCl (1.5 equiv., 0.29 g), HOBt (2.5 equiv., 0.37 g), 5-methoxytryptamine (0.8 equiv. 0.152 g), and DIPEA (2.5 equiv., 0.33 g) were added at room temperature followed by the general procedure as described above.

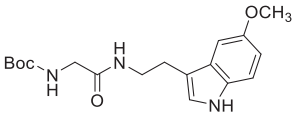

Brown solid powder, yield (0.202 g, 73%). ^{1}H NMR ($CDCl_3$, 500 MHz): δ 10.65 (bs, 1H, –NH), 7.85 (t, $J = 5.5$ Hz, 1H, –NH), 7.21 (d, $J = 9.0$ Hz, 1H, Ar-H), 7.10 (d, $J = 2.0$ Hz, 1H Ar-H), 7.02 (d, $J = 2.0$ Hz, 1H, Ar-H), 6.92 (t, $J = 7.0$ Hz, 1H, Ar-H), 6.70 (dd, $J_1 = 6.0$ Hz, $J_2 = 2.5$ Hz, 1H, Ar-H), 3.71 (s, 3H, —OCH_3), 3.51 (d, $J = 6.5$ Hz, 2H, methylene protons), 2.77 (t, $J = 7.5$ Hz, 2H, methylene protons), 1.38 (s, 9H, Boc protons).

4.1.7.3. tert-butyl (2-((2-(5-chloro-1H-indol-3-yl)ethyl)amino)-2-oxoethyl)carbamate (11c). Into a stirring solution of compound *tert*-butoxycarbonyl)glycine (1 equiv. 0.175 g) in THF (20 mL), EDCI.HCl (1.5 equiv., 0.29 g), HOBt (2.5 equiv., 0.37 g), **5-**chlorotryptamine (0.8 equiv. 0.184 g), and DIPEA (2.5 equiv., 0.33 g) were added at room temperature followed by the general procedure as described above.

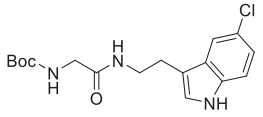

White solid powder, yield (0.254 g, 75%). ^{1}H NMR ($CDCl_3$, 500 MHz): δ 11.03 (bs, 1H, –NH), 7.86 (t, $J = 5.0$ Hz, 1H, –NH), 7.34 (d, $J = 8.5$ Hz, 1H, Ar-H), 7.23 (bs, 1H, Ar-H), 7.05 (dd, $J_1 = 8.5$ Hz, $J_2 = 2.0$ Hz, 1H, Ar-H), 6.93 (t, $J = 6.0$ Hz, 1H, Ar-H), 3.50 (d, $J = 6.0$ Hz, 2H, methylene protons), 3.31 (t, $J = 6.5$ Hz, 2H, methylene protons), 2.78 (t, $J = 7.5$ Hz, 2H, methylene protons), 1.38 (s, 9H, Boc protons).

*4.1.8. General procedure for synthesis of intermediate **12a-12c***

Into a stirring solution of compound **11a-11c** (0.3 g, 1.0 mmol) in methanol (20 mL), ether HCl (3 mL) was added slowly at room temperature, and the reaction mixture was stirred for 12 h. The progress of the reaction was monitored by TLC. After completion of the reaction, the Et_2O (10 mL) was added to provide HCl salt. The HCl salt was further converted to free amine by treatment with Na_2CO_3 solution and extracted with EtOAc (2 × 30 mL). The combined organic layers were dried over Na_2SO_4, and concentrated in vacuo to provide the pure free amine product **12a-12c**, which were subjected to next reaction without further purification.

*4.1.9. (E)-N-(2-((2-(1H-indol-3-yl)ethyl)amino)-2-oxoethyl)-3-(4-hydroxy-3-methoxyphenyl)acrylamide (**13a**)*

Into a stirring solution of compound **FA** (0.3 g, 1.54 equiv.) in THF (20 mL), EDCI.HCl (2.31 equiv., 0.35 g), HOBt (3.86 equiv., 0.52 g), **12a** (0.8 equiv. 0.173 g), and DIPEA (2.5 equiv., 0.33 g) were added at room temperature followed by the general procedure as described above. The crude material was purified by column chromatography using silica gel (100–200 mesh size) as a stationary phase with help of EtOAc:hexane (9:1) as mobile phase.

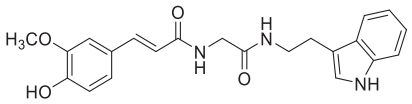

Brown solid powder, (0.152 g, 71% yield). ^{1}H NMR (DMSO-d_6, 500 MHz): δ 10.78 (bs, 1H —OH), 9.44 (bs, 1H, –NH), 8.14 (t, $J = 6.0$ Hz, 1H, –NH), 8.01 (t, $J = 6.0$ Hz, 1H, –NH), 7.53 (d, $J = 8.0$ Hz, —CH═CH—), 7.35–7.31 (m, 2H, Ar-H), 7.14 (t, $J = 4.5$ Hz, 2H, Ar-H), 7.06–6.95 (m, 3H, Ar-H), 6.79 (d, $J = 8.0$ Hz, 1H, Ar-H), 6.56 (d, $J = 15.5$ Hz, 1H, —CH═CH—), 3.80–3.78 (m, 5H, —OCH_3 and methylene protons), 3.34 (s, 2H, merge with DMSO-d_6 methylene protons), 2.82 (t, $J = 7.5$ Hz, 2H, methylene protons). ^{13}C NMR (DMSO-d_6, 126 MHz): δ 169.2, 166.1, 148.7, 148.2, 139.8, 136.6, 127.6, 126.8, 123.0, 122.0, 121.3, 119.2, 118.6, 116.1, 112.1, 111.8, 111.3, 56.0, 42.7, 25.6. ESI-HRMS for $C_{22}H_{23}N_3O_4$. $(M+H)^+$ calcd. 394.1767, found 394.1773.

*4.1.10. (E)-3-(4-hydroxy-3-methoxyphenyl)-N-(2-((2-(5-methoxy-1H-indol-3-yl)ethyl)amino)-2-oxoethyl)acrylamide (**13b**)*

Into a stirring solution of compound **FA** (0.3 g, 1.54 equiv.) in THF (20 mL), EDCI.HCl (2.31 equiv., 0.35 g), HOBt (3.86 equiv., 0.52 g), **12b** (0.8 equiv. 0.197 g), and DIPEA (2.5 equiv., 0.33 g) were added at room temperature followed by the general procedure as described above.

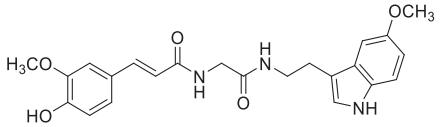

White solid powder, (0.158 g, 66% yield). ^{1}H NMR (DMSO-d_6, 500 MHz): δ 10.65 (bs, 1H —OH), 9.44 (bs, 1H, –NH), 8.15 (t, $J = 6.0$ Hz 1H, –NH), 8.03 (t, $J = 6.0$ Hz, 1H, –NH), 7.35 (d, $J = 16.0$ Hz, 1H, Ar-H), 7.22 (d, $J = 9.0$ Hz, 1H, Ar-H), 7.13 (dd, $J_1 = 6.5$ Hz, $J_2 = 2.0$ Hz, 2H, Ar-H), 7.03–7.01 (m, 2H, Ar-H), 6.80 (d, $J = 8.0$ Hz, 1H, Ar-H), 6.71 (dd, $J_1 = 6.5$ Hz, $J_2 = 2.0$ Hz, 1H, Ar-H), 6.58 (d, $J = 16.0$ Hz, 1H, —CH═CH—), 3.81 (s, 5H, FA —OCH_3 and —CH_2-), 3.76 (s, 3H, —OCH_3), 3.36 (t, $J = 6.0$ Hz, 2H, —CH_2-), 2.80 (t, $J = 7.5$ Hz, 2H, —CH_2-). ^{13}C NMR (DMSO-d_6, 126 MHz): δ 169.2, 166.1, 153.4, 148.7, 148.2, 139.7, 131.8, 127.9, 126.8, 123.8, 122.0, 119.2, 116.1, 112.4, 111.9, 111.5, 111.3, 100.5, 55.9, 55.8, 42.7, 41.9, 25.7. ESI-HRMS for $C_{23}H_{25}N_3O_5$. $(M+H)^+$ calcd. 424.1872, found 424.1874.

*4.1.11. (E)-N-(2-((2-(5-chloro-1H-indol-3-yl)ethyl)amino)-2-oxoethyl)-3-(4-hydroxy-3-methoxyphenyl)acrylamide (**13c**)*

Into a stirring solution of compound **FA** (0.3 g, 1.54 equiv.) in THF (20 mL), EDCI.HCl (2.31 equiv., 0.35 g), HOBt (3.86 equiv., 0.52 g), **12c** (0.8 equiv. 0.201 g), and DIPEA (2.5 equiv., 0.33 g) were added at room temperature followed by the general procedure as described above.

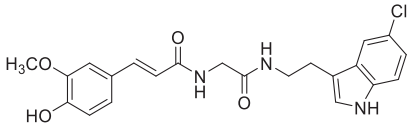

White solid powder, (0.167 g, 69% yield). ^{1}H NMR (DMSO-d_6, 500 MHz): δ 11.03 (s, 1H —OH), 9.52 (s, 1H, –NH), 8.18 (t, $J = 6.0$ Hz, 1H, –NH), 8.04 (t, $J = 6.0$ Hz, 1H, –NH), 7.59 (d, $J = 2.0$ Hz, 1H, Ar-H), 7.37–7.34 (m, 2H, Ar-H), 7.25 (d, $J = 2.0$ Hz, 1H, Ar-H), 7.05 (dd, $J_1 = 6.0$ Hz, $J_2 = 2.0$ Hz, 2H, Ar-H), 6.80 (d, $J = 8.0$ Hz, 1H, Ar-H), 6.57 (d, $J = 16.0$ Hz, 1H, Ar-H), 3.81 (s, 5H, —OCH_3 and methylene protons), 3.34–3.32 (m, 4H merged with DMSO-d_6 methylene protons), 2.80 (t, $J = 7.5$ Hz, 2H, methylene protons). ^{13}C NMR (DMSO-d_6, 126 MHz): δ 169.3, 166.2, 148.8, 148.3, 139.8, 135.1, 128.8, 126.8, 125.1, 123.4, 122.0, 121.2, 119.2, 117.9, 116.1, 113.3, 112.1, 111.3, 67.4, 56, 42.7, 25.4. ESI-HRMS for $C_{21}H_{23}ClN_2O_3$. $(M+H)^+$ calcd. 428.1377, found 428.1376.

4.2. Biology

4.2.1. Inhibition of cholinesterase (hAChE and eqBChE)

AChE (*h*AChE, from human erythrocytes, CAS No. 9000–81-1), butyrylcholinesterase (*eq*BChE, from equine serum, CAS No. 9001–08-5), 5, 5′-dithiobis- 2-nitrobenzoic acid (DTNB-Ellman's reagent, CAS No. 69–78-3), acetylthiocholine iodide (ATCI, CAS No. 1866–15-5), butyrylthiocholine iodide (BTCI, CAS No. 1866–16-6) and **FA** (CAS No. 1261170–81-3) were purchased form Sigma Aldrich. Donepezil hydrochloride (**DPZ**.HCl) (Sigma Aldrich, CAS No. 1261170–81-3) was used as reference. The ChE inhibitory property of all the synthesized derivatives was performed using the Ellman colorimetric method with slight modification.[26] Briefly, 50 μL of *h*AChE (0.022 U/mL) or 50 μL of BChE (0.06 U/mL) was incubated with 10 μL of test or standard compound at 37 °C for 30 min. Further, 30 μL of the substrate, viz. ATCI (1.5 mM) or BTCI (15 mM) was added, and the solution was incubated for additional 30 min. Finally, 160 μL of 0.15 mM DTNB (for *h*AChE) or 160 μL of 1.5 mM DTNB (for *eq*BChE) were added into it and the absorbance was measured at 415 nm wavelength using Synergy™ HT and Epoch 2, Bio-Tek Instruments, Inc (microplate reader). Results are expressed as the mean ± SD of at least two/three different experiments performed in triplicate. The inhibition percent was calculated by the following expression:$\%\text{inhibition} = [(\text{Ac} - \text{Ai})/\text{Ac}]\text{X}100$. Where Ai and Ac are the absorbance obtained for AChE or BChE in the presence and absence of inhibitors.

4.2.2. DPPH antioxidant assay

DPPH (2,2-diphenyl-1-picryl-hydrazyl-hydrate) radical method is an antioxidant assay based on reduction of DPPH to a yellow-colored diphenylpicrylhydrazine. 2,2-Diphenyl-1-picrylhydrazyl (DPPH; CAS No. 1898–66-4) was purchased from Sigma-Aldrich, India. All the assays were carried out in extra pure methanol. Briefly, 75 μL of different concentrations of test compounds were added to a 96 well plate. To this 75 μL of DPPH (200 μM) solution was added. Finally, 96 well microplate was incubated at 37 °C for 25 min on thermomixer with moderate shaking at 300 rpm. The absorbance was measured at 517 nm wavelength using Epoch 2 microplate reader, Bio-Tek Instruments, Inc. The activity of **FA**, a recognized antioxidant was used as a standard. The radical-scavenging activity was determined by the equation. $\%Inhibition = [(absorbance\ of\ control - absorbance\ of\ test)absorbance\ of\ control] \times 100.$

All the experiments were performed in duplicate or triplicate.

4.2.3. Enzyme kinetic studies

The enzyme kinetic studies were performed in order to investigate the binding kinetics of ligand with the enzyme (AChE and BChE). The kinetics study was performed as per the previously reported method.[26] Briefly, 50 μL of enzyme (*h*AChE or *eq*BuChE) was preincubated with the test compounds at 37 °C for 30 min, followed by the addition of substrate ATCI (0.5, 1.0, 1.5, 2.0 and 2.5 mM), or BTCI (5, 10, 15, 20 and 25 mM). Finally, 160 μL of 5,5′-dithiobis- 2-nitrobenzoic acid (DTNB-Ellman's reagent, 0.15 mM (for AChE) or 1.5 mM (for BChE) was added into it, and the absorbance was recorded at 415 nm using Epoch 2 microplate reader, Bio-Tek Instruments, Inc. Each experiment was performed in duplicate.

4.2.4. PAS binding assay

The affinity of compound for the PAS of AChE was examined by propidium iodide, a known PAS-specific ligand of AChE. Propidium iodide (CAS No. 25535–16-4) was purchased from Sigma-Aldrich. All the assays were carried out in Tris-HCl buffer (pH 8.0) and the measurements were carried out in 200 μL solution volume in 96-well plates. Briefly, 75 μL of 5 U/ml *h*AChE was incubated, for 6 h at 25 °C, with a 75 μL solution of the compound (50, 20, 10 and 5 μM final concentration) or **DPZ** as positive control, respectively. Finally, the sample were incubated for 20 min with propidium iodide (50 μL of 20 μM), and the fluorescence was measured using Synergy™ HT, Bio-Tek Instruments, Inc. microplate reader. Wavelengths of excitation and emission were 535 and 595 nm, respectively. Each assay was repeated at least, at two different times.

4.2.5. Molecular docking

The 3D crystal structures of *h*AChE in complex with DPZ (PDB ID-4EY7) and *h*BChE in complex with tacrine (PDB ID-4BDS) were retrieved from the Brookhaven protein data bank.[13,42] Protein Preparation Wizard of Schrödinger software package (Schrödinger, LLC, New York, NY) was used to prepare both proteins. This step includes removal of water beyond 5 Å from the HET group, addition of missing hydrogen, optimization of orientations of hydroxyl and amino groups, assignment of right bond orders, and the determination of ionization of amino acids using ProtAssign utility. The resulting structures were further subjected to restrained minimization with cutoff root mean square deviation (RMSD) of 0.3 Å. Finally, the prepared complexes were further used for molecular docking and MD simulation study. All the small molecules were drawn using 2D sketcher and were subjected to ligand preparation using the LigPrep module of Schrödinger software package (Schrödinger, LLC, New York, NY). The different possible ionization states for ligands were generated at the physiological pH (7.0 ± 2), and OPLS3 force field was used to minimize the ligands. Two different grids, one for the AChE (4EY7) and other for the BChE (4BDS) were prepared using the centroid of bound co-crystallized ligands. The both grids were standardized by re-docking the co-crystallized ligands *i.e.* **DPZ** and tacrine to AChE and BChE, respectively. Finally, docking of all ligands was performed by the Glide module of the Schrödinger software package (Schrödinger, LLC, New York, NY) using standard operating procedures with the extra precision (XP) protocol.[43]

4.2.6. Molecular dynamics simulations

All-atom MD simulations were performed using the Desmond-v6.1 module of Schrödinger Software Package (Schrödinger, LLC, New York, NY).[44] The system builder panel was used to prepare the initial systems for MD simulations. The apo-AChE, apo-BChE and all docked complexes were placed in a cubic box of 1.0 nm size. The boxes were solvated with TIP3P water models and charged systems were neutralized using counter ions (Na^+ or Cl^- ions).[45] An ionic strength of 0.15 M was maintained by adding Na^+ and Cl^- ions to all the systems. Further, the solvated systems were minimized and equilibrated under NPT ensemble using the default protocol of Desmond. It includes a total of nine stages, among which there are two minimization and four short simulations (equilibration phase) steps.[46,47] All minimized and equilibrated systems were subjected to MD run with periodic boundary conditions in NPT ensemble using OPLS_2005 force field parameter for 100 ns.[48] During the simulation, the pressure (1 atm) and temperature (300 K) of the systems were maintained by Martyna–Tobias–Klein barostat and Nose–Hoover Chain thermostat, respectively.[49,50] The binding energy between the AChE/BChE and ligands (3k & 13b) was calculated using the inbuilt script thermal_mmgbsa.py.[51] The binding energy was calculated from the last 25 ns of trajectory at an interval of 50 ps for all four (AChE-**3k**, AChE-**13b**, BChE-**3k**, and BChE-**13b**) systems. The solvent accessibility surface area (SASA) of AChE/BChE in the presence of different ligands was also calculated using the script binding_sasa.py.

4.2.7. Metal chelation

The metal chelation was monitored spectrophotometrically using Epoch 2 microplate reader, Bio-Tek Instruments, Inc. Iron (III) chloride hexahydrate ($FeCl_3{\cdot}6H_2O$, CAS No. 10025–77-1) was purchased form Sigma Aldrich (USA). The stock solution of compound **13b** (600 μM) was prepared in extra pure methanol. Compound **13b** was then diluted in methanol to make a 300 μM solution and the solution was kept aside for absorbance reading on next day from 300 to 700 nm. $FeCl_3{\cdot}6H_2O$ was next dissolved in methanol to make a 600 μM light orange solution. The two solutions [**13b** (600 μM) and $FeCl_3{\cdot}6H_2O$ (600 μM)] were mixed

together in equal volume, which gave a light-yellow solution. Finally, the sample solution was incubated at 25 °C for 24 h on thermomixer with vigorous shaking at 1000 rpm. After 24 h, the solution color changed from yellow to blue, and was subjected to UV scan. Finally, the pH of the solution was maintained to 7.4 by adding base diisopropylethylamine (DIPEA) (diluted with water) which produced a deep-blue color which was followed by UV spectra scan. Each concentration was assayed in duplicate.

The molar ratio method was performed in order determine the stoichiometry of the **13b**-Fe (III) complex by titrating the solution of compound **13b** with $FeCl_3$ solution (at different molar ratio). The UV spectra were recorded at room temperature. The absorbance spectrum represents the formation of new absorption band, indicating that compound can interact with Fe (III) ions. Thereafter, the mole fraction of Fe (III) and absorbance of **13b** was plotted to obtain stoichiometry of complex.

4.2.8. Assessment of cell viability by MTT assay

The cytotoxicity of **13b** on n2a cells was determined by MTT assay following our earlier publications. Briefly, Neuro2a cells were seeded at a concentration of 1×10^4 cells/well in 96 well plates and were incubated overnight for adherence. The compound, **13b** was added in N2a cells at a concentration of 20, 10, 5, 2.5, 1, 0.1 and 0.01 μM in triplicates and incubated for 24 h at 5% CO_2 at 37 °C followed by MTT assay.

*4.2.9. Effect of compound **13b** on H_2O_2 induced cell death*

The H_2O_2-induced cellular damage model of neurodegenerative disorder in n2a cell line was established to evaluate the protective effect of **13b**. The cells were seeded at a density of 1×10^4 cells/well into 96-well plates and incubated for overnight. Next, the cells were treated with 100, 200, 400, 600, and 800 μM of H_2O_2 for 24 h, and control wells were cultured without any treatment. Following the treatment, 3-(4,5-dimethylthiazol-2-yl)-2,5-diphenyltetrazolium bromide (MTT) reagent was added and incubated at 37 °C for 4 h. Next, the solution in the wells was replaced by the extraction buffer (0.04 N HCl in isopropanol), followed by additional incubation at 37 °C for 1 h in dark and the optical densities was measured at 570 nm using multimode microplate reader (Infinite® 200 PRO, TECAN.). Each experiment was repeated at least in triplicate. The MTT assay was also used to determine the protective effect of **13b** in H_2O_2-induced cell damage based on the evaluation of cell viability. The results were also confirmed by microscopic observation. The n2a cells were seeded at a density of 1×10^4 cells/well into 96-well plates and incubated for overnight. Next, the cells were grown in the presence or absence of different concentrations (1, 2.5, 5, 10 or 20 μM) of **13b** for 24 h, then further co-incubated with 600 μM H_2O_2 for another 24 h. The cells in the control group were cultured without any treatment. Each experiment was repeated at least in triplicate. Post-treatment, MTT was added to all of the cells seeded wells and incubated at 37 °C for 4 h followed by a general procedure described above. Percent cell viability was calculated by the formula

$$\text{Percentage of viability} = \frac{\text{Mean OD value of experimental sample (treated)}}{\text{Mean OD value of experimental control (untreated)}} \times 100$$

4.2.10. Parallel artificial membrane permeability assay

The blood–brain barrier penetration assay of the developed molecules was performed using the parallel artificial membrane permeation assay (PAMPA) described by Di *et al.* Five commercial drugs such as testosterone (CAS No. 58–22-0), hydrocortisone (CAS No. 50–23-7), and corticosterone (CAS No. 50–22-6) were purchased from TCI chemicals. The PAMPA kit (Cat # PAMPA 096, Lot No. BJ07A12), including the donor microplate (PVDF membrane, pore size 0.45 mm) and acceptor microplates, were purchased from Bioassay systems Pvt. Ltd. Porcine brain lipid (PBL, CAS No. 86088–88-2, Lot No. 141101P-100MG-A-079) and *n*-dodecane (CAS No. 112–40-3) were purchased from Avanti Polar Lipids and Avra Synthesis, respectively. All the experiments were carried out in phosphate buffer saline (PBS, pH 7.4).

4.2.10.1. Preparation of the stock solution. The stock solution (10 mM) of test or standard compounds were prepared in molecular biology grade DMSO (for poor solubility, MeOH was used). 500 μL of 500 μM test compound was prepared *via* dissolving 25 μL of stock solution of test compounds in 475 μL PBS (pH 7.4). Similarly, 500 μL of 500 μM of the standard control was prepared in PBS (pH 7.4). 200 μL of equilibrium standard of each of the test and standard compound was prepared *via* dissolving 80 μL of 500 μM of test and standard compound with 120 μL PBS. 250 μL blank control was prepared via dissolving 5 μL DMSO in 245 μL PBS. Set aside the equilibrium standard and blank control for analysis the next day.

4.2.10.2. Procedure. The acceptor plate well was filled with 300 μL of PBS buffer. The filter membrane of the donor (top) plate was coated with 5 μL of BBB-specific lipid solution prepared via dissolving 20 mg of PBL in 600 μL of *n*-dodecane. Be careful not to puncture the membrane with the tip of pipette. After 30 min, add 200 μL of each of the test (500 μM) and standard compound (500 μM) to duplicate wells in donor plate. The donor plate was kept carefully into the acceptor plate wells like a sandwich and incubated for 18 h at 37 °C in a moistened sealed bag to prevent evaporation. Carefully remove donor plate and concentrations of drug in the acceptor, equilibrium standard for each test compounds, and permeability control along with blank control were determined by UV spectroscopy (Epoch 2 micrplate reader, BioTek, USA) *via* placing 100 μL solution to the well of 96-well micro test plate. Read absorbance spectrum from 200 nm to 500 nm in 10 nm interval to determine the absorbance of the test compound. Each experiment was performed in duplicate. P_e was calculated using the following expression: $Pe = C \times -\ln(1- OD_A/OD_E)$ cm/s, where OD_A = absorbance of Acceptor solution, OD_E is the absorbance of equilibrium standard, and if the experiment is running for 18 hrs, then $C = 7.72 \times 10^{-6}$. The results are given as the mean ± SD.

4.2.11. In-Vivo experiments

4.2.11.1. Animals. 3 months old male C57BL6 mice, 25–30 gm each, were obtained from the Breeding unit of small animal Facility and acclimatized in an experimental small animal facility for 5 days (12 h light/dark cycle, temperature 25 ± 2 °C) at National Institute of Immunology, New Delhi). Mice were supplied with commercial food granules and sterilized water unless otherwise stated. All the methods and procedures performed in this study were following the guidelines approved (IAEC# 565/20) by the Institutional Animal ethical committee of National institute of Immunology, New Delhi.

4.2.11.2. Drugs and chemicals. The compound **13b** was suspended in 20 μL DMSO and volume makes up by the phosphate-buffered saline (pH 7.4), and donepezil hydrochloride & scopolamine hydrochloride was

dissolved in water to carry out the *in-vivo* studies.

4.2.12. Morris water maze

Adult C57BL6 mice (25–30 g) were divided into five different groups (7 animals each) according to their treatment (i) normal control, (ii) scopolamine, (iii) DPZ 0.5 mg/kg with scopolamine, (iv) **13b** at 5 mg/kg with scopolamine, and (v) **13b** at 10 mg/kg with scopolamine. Scopolamine hydrochloride (1 mg/kg) was administered intraperitoneally (*i.p.*) to the animals of all groups except the control group, which received an equal volume of PBS, respectively. Donepezil hydrochloride (0.5 mg/kg i.p.) and **13b** (5 and 10 mg/kg) was administered orally (*p.o.*) 30 min before administration of scopolamine to the respective group of animals for 14 days. From 10 to 14th days of the treatment period, learning and memory test were performed using the Morris water maze (MWM) test. It consisted of a circular tank of 100 cm in diameter. The tank was divided into four quadrants and labelled as A, B, C and D. The quadrant in which the platform is placed is known as target quadrant/zone. Before the actual trials mice were trained to find the hidden platform, three trials per day for 4 days. During the training period, the mice were allowed to swim freely for 60 s to find the hidden platform and to show them that, there is a place in a pool where they can come and rescue themselves. Upon the actual start of the testing, the transparent platform was placed 1.5 cm below the water level. Animals were given three trials per day for 4 days consecutively. The escape latency was recorded, which is defined as the total time taken (*sec*) to reach the platform in 4 consecutive days. On 5th day, probe test was performed in which platform was removed and the animal was allowed to swim freely for 60 s to calculate the total time spent in the target quadrant. All the monitoring was done using video tracking system attached to computer and recorded with software. Data were analyzed using ANY maze software (Stoeling Co., USA). Throughout the experiment, the temperature of the pool (25 ± 2 °C) and the area of the platform were maintained constant.

Funding

This work is supported by Science and Engineering Research Board under Core Research Grant (SERB-CRG/2018/003490) and Indian Institute of Technology (BHU) (SM/2016–17/1198/L). Y.P.S., G.S. are thankful to Indian Institute of Technology (BHU) and MHRD, India for fellowship. The work is supported by core grant of national institute of Immunology, India to SG, KK, and SJ is thankful to NII for fellowship. PU is thankful for the young scientist fellowship funding support from the Department of Health Research, Ministry of Health and Family Welfare, Govt of India (#12014/20/2018-HR).

Declaration of Competing Interest

The authors declare that they have no known competing financial interests or personal relationships that could have appeared to influence the work reported in this paper.

Acknowledgments

GM is thankful to the Central Instrument Facility (CIF) Indian Institute of Technology (BHU) for providing NMR and AFM facilities. GM is also thankful to Indian Institute of Technology, Ropar, CSIR-North East Institute of Science and Technology and CSIR- Indian Institute of Chemical Technology, Hyderabad for the HRMS study.

Appendix A. Supplementary material

Supplementary data to this article can be found online at https://doi.org/10.1016/j.bmc.2021.116385.

References

[1] Raji CA, Lopez OL, Kuller LH, Carmichael OT, Becker JT. Age, Alzheimer disease, and brain structure. *Neurology*. 2009;73:1899–1905.
[2] 2019 Alzheimer's disease facts and figures, Alzheimer's & Dement 15 (2019) 321–387.
[3] WHO, 2020. https://www.who.int/news-room/fact-sheets/detail/dementia.
[4] Singh YP, Rai H, Singh G, et al. A Review on Ferulic Acid and Analogs Based Scaffolds for the Management of Alzheimer's Disease. *Eur J Med Chem*. 2021;215:113278. https://doi.org/10.1016/j.ejmech.2021.113278.
[5] Kumar D, Ganeshpurkar A, Kumar D, Modi G, Gupta SK, Singh SK. Secretase inhibitors for the treatment of Alzheimer's disease: Long road ahead. *Eur J Med Chem*. 2018;148:436–452.
[6] Singh YP, Pandey A, Vishwakarma S, Modi G. A review on iron chelators as potential therapeutic agents for the treatment of Alzheimer's and Parkinson's diseases. *Mol Diversity*. 2019;23(2):509–526.
[7] Patel DV, Patel NR, Kanhed AM, et al. Novel Multitarget Directed Triazinoindole Derivatives as Anti-Alzheimer Agents. *ACS Chem Neurosci*. 2019;10(8):3635–3661.
[8] Gerenu G, Liu K, Chojnacki JE, et al. Curcumin/Melatonin Hybrid 5-(4-Hydroxyphenyl)-3-oxo-pentanoic Acid [2-(5-Methoxy-1H-indol-3-yl)-ethyl]-amide Ameliorates AD-Like Pathology in the APP/PS1 Mouse Model. *ACS Chem Neurosci*. 2015;6(8):1393–1399.
[9] Albertini C, Salerno A, de Sena Murteira P, Pinheiro MLB. From combinations to multitarget-directed ligands: A continuum in Alzheimer's disease polypharmacology. *Med Res Rev*. 2020.
[10] Craig LA, Hong NS, McDonald RJ. Revisiting the cholinergic hypothesis in the development of Alzheimer's disease. *Neurosci Biobehav Rev*. 2011;35(6):1397–1409.
[11] Terry Jr AV, Buccafusco JJ. The cholinergic hypothesis of age and Alzheimer's disease-related cognitive deficits: recent challenges and their implications for novel drug development. *The Journal of pharmacology and experimental therapeutics*. 2003;306:821–827.
[12] H. Ferreira-Vieira T, M. Guimaraes I, R. Silva F, M. Ribeiro F. Alzheimer's disease: Targeting the Cholinergic System. *Curr Neuropharmacol*. 2016;14(1):101–115.
[13] Cheung J, Rudolph MJ, Burshteyn F, et al. Structures of human acetylcholinesterase in complex with pharmacologically important ligands. *J Med Chem*. 2012;55:10282–10286.
[14] Cheung J, Rudolph MJ, Burshteyn F, et al. Structures of human acetylcholinesterase in complex with pharmacologically important ligands. *J Med Chem*. 2012;55:10282–10286.
[15] Sawatzky E, Wehle S, Kling B, et al. Discovery of Highly Selective and Nanomolar Carbamate-Based Butyrylcholinesterase Inhibitors by Rational Investigation into Their Inhibition Mode. *J Med Chem*. 2016;59:2067–2082.
[16] Unzeta M, Esteban G, Bolea I, et al. Multi-Target Directed Donepezil-Like Ligands for Alzheimer's Disease. *Front Neurosci*. 2016;10. https://doi.org/10.3389/fnins.2016.00205.
[17] Mushtaq G, Greig NH, Khan JA, Kamal MA. Status of acetylcholinesterase and butyrylcholinesterase in Alzheimer's disease and type 2 diabetes mellitus. *CNS Neurol Disord Drug Targets*. 2014;13:1432–1439.
[18] Dighe SN, Deora GS, De la Mora E, et al. Discovery and Structure-Activity Relationships of a Highly Selective Butyrylcholinesterase Inhibitor by Structure-Based Virtual Screening. *J Med Chem*. 2016;59:7683–7689.
[19] Uttara B, Singh AV, Zamboni P, Mahajan RT. Oxidative stress and neurodegenerative diseases: a review of upstream and downstream antioxidant therapeutic options. *Curr Neuropharmacol*. 2009;7:65–74.
[20] Andersen JK. Oxidative stress in neurodegeneration: cause or consequence? *Nat Med*. 2004;10(S7):S18–S25.
[21] Gleason A, Bush AI. Iron and Ferroptosis as Therapeutic Targets in Alzheimer's Disease. *Neurotherapeutics*. 2021;18(1):252–264.
[22] Bush AI. The metallobiology of Alzheimer's disease. *Trends Neurosci*. 2003;26:207–214.
[23] Praticò D. Oxidative stress hypothesis in Alzheimer's disease: a reappraisal. *Trends Pharmacol Sci*. 2008;29(12):609–615.
[24] Zhao Y, Zhao B. Oxidative stress and the pathogenesis of Alzheimer's disease. *Oxid Med Cell Longev*. 2013;2013:316523.
[25] Smith MA, Rottkamp CA, Nunomura A, Raina AK, Perry G. Oxidative stress in Alzheimer's disease. *Biochimica et Biophysica Acta (BBA) - Mol Basis Dis*. 2000;1502:139–144.
[26] Singh YP, Tej GNVC, Pandey A, et al. Design, synthesis and biological evaluation of novel naturally-inspired multifunctional molecules for the management of Alzheimer's disease. *Eur J Med Chem*. 2020;198:112257. https://doi.org/10.1016/j.ejmech.2020.112257.
[27] Fusco D, Colloca G, Lo Monaco MR, Cesari M. Effects of antioxidant supplementation on the aging process. *Clin Interv Aging*. 2007;2:377–387.
[28] Devasagayam TP, Tilak JC, Boloor KK, Sane KS, Ghaskadbi SS, Lele RD. Free radicals and antioxidants in human health: current status and future prospects. *The Journal of the Association of Physicians of India*. 2004;52:794–804.
[29] Poprac P, Jomova K, Simunkova M, Kollar V, Rhodes CJ, Valko M. Targeting Free Radicals in Oxidative Stress-Related Human Diseases. *Trends Pharmacol Sci*. 2017;38(7):592–607.
[30] Wang Lu, Yin Y-L, Liu X-Z, et al. Current understanding of metal ions in the pathogenesis of Alzheimer's disease. *Transl Neurodegener*. 2020;9(1). https://doi.org/10.1186/s40035-020-00189-z.
[31] Gella A, Durany N. Oxidative stress in Alzheimer disease. *Cell Adh Migr*. 2009;3(1):88–93.

[32] Newman DJ, Cragg GM. Natural Products as Sources of New Drugs from 1981 to 2014. *Journal of Natural Products*. 2016;79:629–661.
[33] Sang Zhipei, Pan Wanli, Wang Keren, et al. Design, csyncthesis and evaluation of novel ferulic acid-O-alkylamine derivatives as potential multifunctional agents for the treatment of Alzheimer's disease. *Eur J Med Chem*. 2017;130:379–392.
[34] Sang Zhipei, Wang Keren, Bai Ping, et al. Design, synthesis and biological evaluation of novel O-carbamoyl ferulamide derivatives as multi-target-directed ligands for the treatment of Alzheimer's disease. *Eur J Med Chem*. 2020;194: 112265. https://doi.org/10.1016/j.ejmech.2020.112265.
[35] Ellman George L. Tissue sulfhydryl groups. *Arch Biochem Biophys*. 1959;82(1): 70–77.
[36] Cheng F, Li W, Zhou Y, et al. admetSAR: A Comprehensive Source and Free Tool for Assessment of Chemical ADMET Properties. *J Chem Inf Model*. 2012;52:3099–3105.
[37] Di L, Kerns EH, Fan K, McConnell OJ, Carter GT. High throughput artificial membrane permeability assay for blood-brain barrier. *Eur J Med Chem*. 2003;38: 223–232.
[38] D'Hooge R, De Deyn PP. Applications of the Morris water maze in the study of learning and memory. *Brain Res Rev*. 2001;36:60–90.
[39] Dudchenko PA. An overview of the tasks used to test working memory in rodents. *Neurosci Biobehav Rev*. 2004;28:699–709.
[40] Boutin S, Maltais R, Roy J, Poirier D. Synthesis of 17β-hydroxysteroid dehydrogenase type 10 steroidal inhibitors: Selectivity, metabolic stability and enhanced potency. *Eur J Med Chem*. 2021;209, 112909.
[41] Mehanna AS, Kim JY. Design, synthesis, and biological testing of thiosalicylamides as a novel class of calcium channel blockers. *Bioorg Med Chem*. 2005;13: 4323–4331.
[42] Nachon F, Carletti E, Ronco C, et al. Crystal structures of human cholinesterases in complex with huprine W and tacrine: elements of specificity for anti-Alzheimer's drugs targeting acetyl- and butyryl-cholinesterase. *Biochem J*. 2013;453:393–399.
[43] Friesner RA, Murphy RB, Repasky MP, et al. Extra Precision Glide: Docking and Scoring Incorporating a Model of Hydrophobic Enclosure for Protein−Ligand Complexes. *J Med Chem*. 2006;49:6177–6196.
[44] John A, Umashankar V, Krishnakumar S, Deepa PR. Comparative Modeling and Molecular Dynamics Simulation of Substrate Binding in Human Fatty Acid Synthase: Enoyl Reductase and β-Ketoacyl Reductase Catalytic Domains. *Genomics Inform*. 2015;13:15–24.
[45] Mark P, Nilsson L. Structure and Dynamics of the TIP3P, SPC, and SPC/E Water Models at 298 K. *The Journal of Physical Chemistry A*. 2001;105:9954–9960.
[46] Gahlawat A, Kumar N, Kumar R, et al. Structure-Based Virtual Screening to Discover Potential Lead Molecules for the SARS-CoV-2 Main Protease. *J Chem Inf Model*. 2020;60:5781–5793.
[47] Kumar N, Gahlawat A, Kumar RN, Singh YP, Modi G, Garg P. Drug repurposing for Alzheimer's disease: in silico and in vitro investigation of FDA-approved drugs as acetylcholinesterase inhibitors. *J Biomol Struct Dyn*. 2020:1–15.
[48] Cho K, Joannopoulos JD, Kleinman L. Constant-temperature molecular dynamics with momentum conservation. *Phys Rev E*. 1993;47:3145–3151.
[49] Genheden S, Kuhn O, Mikulskis P, Hoffmann D, Ryde U. The Normal-Mode Entropy in the MM/GBSA Method: Effect of System Truncation, Buffer Region, and Dielectric Constant. *J Chem Inf Model*. 2012;52:2079–2088.
[50] Nosé S. A unified formulation of the constant temperature molecular dynamics methods. *J Chem Phys*. 1984;81:511–519.
[51] Lyne PD, Lamb ML, Saeh JC. Accurate prediction of the relative potencies of members of a series of kinase inhibitors using molecular docking and MM-GBSA scoring. *J Med Chem*. 2006;49:4805–4808.